# A unified fidelity-based framework for quantum speed limits in open quantum systems

Tristán M. Osán, 1,2,\* Yanet Alvarez, 3,4 Mariela Portesi, 3,4 and Pedro W. Lamberti<sup>2,5</sup>

<sup>1</sup>Instituto de Física Enrique Gaviola (IFEG-UNC-CONICET),
Universidad Nacional de Córdoba, Av. Medina Allende s/n,
Ciudad Universitaria. (CP:X5000HUA) Córdoba. Argentina
<sup>2</sup>Universidad Nacional de Córdoba. Facultad de Matemática, Astronomía,
Física y Computación. Grupo de teoría de la materia condensada. Av. Medina Allende s/n,
Ciudad Universitaria. (CP:X5000HUA) Córdoba. Argentina

<sup>3</sup>Instituto de Física La Plata (IFLP, CONICET-UNLP). Diag. 113 entre 63 y 64. La Plata (CP:1900). Buenos Aires. Argentina. <sup>4</sup>Universidad Nacional de La Plata. Facultad de Ciencias Exactas. Calle 115 y 47. La Plata (CP:1900). Buenos Aires. Argentina. <sup>5</sup>Consejo Nacional de Investigaciones Científicas y Técnicas (CONICET). Av. Medina Allende s/n,

Ciudad Universitaria. (CP:X5000HUA) Córdoba. Argentina.

In this work, we investigate the role of functionals of generalized fidelity measures in deriving quantum speed limits (QSLs) within a geometric approach. We establish a general theoretical framework and show that, once a specific generalized fidelity is selected, the resulting Margolus–Levitin and Mandelstam–Tamm QSLs for both unitary and nonunitary (Lindblad-type) dynamics depend solely on the chosen fidelity measure. We prove that any monotone, differentiable reparametrization of the chosen fidelity yields exactly the same Margolus–Levitin and Mandelstam–Tamm-type QSL, rendering the QSLs invariant under such transformations and thereby unifying fidelity- and metric-induced geometric formulations. This result highlights the limitations of improving QSLs through functional transformations of fidelity and indicates that genuine improvements must arise from alternative fidelity definitions. We further show that several QSLs reported in the literature are encompassed by our framework and discuss possible extensions based on other generalized fidelity measures beyond those explicitly analyzed. In addition, we consider the damped Jaynes–Cummings model as a concrete physical setting to explore the behavior of the QSLs discussed in this work and analyze their regime-dependent features.

## I. INTRODUCTION

A quantum computer, or any system that processes quantum information, may be viewed more fundamentally as a quantum system that evolves from a given initial state to a physically distinguishable final state under a prescribed set of operations. A natural requirement is that the rate of change of the quantum state should be as fast as possible, both to minimize the total processing time and to limit the exposure of the quantum system to uncontrollable interactions with its environment, which may lead to undesirable phenomena such as decoherence. Notably, quantum physics imposes fundamental limits on the rate at which a quantum state can evolve. These limits are known as quantum speed limits (QSLs). The problem of evaluating the QSL in systems evolving according to certain established dynamics has been a subject of research since the early years of quantum theory. For example, in the case of isolated quantum systems, quantum speed limits such as those of Mandelstam and Tamm (MT) and Margolus and Levitin (ML) set bounds on the minimum time required for a system to evolve from a given initial state to an orthogonal quantum state [1–8]. However, in realistic quantum processes one often aims not to reach an orthogonal state, but rather to drive the system toward an arbitrary, possibly nonorthogonal, target state. Motivated by this idea, several studies have extended the original OSL framework to account for unitary evolution between non-orthogonal states (see, for example, Refs. [9-14]).

Over the past decade, various approaches have extended QSLs beyond idealized closed dynamics to mixed states and open systems using, for example, similarity measures such as Bures fidelity, relative purity, and Fisher-information-based distances [15–18]. Each approach has illuminated a different aspect of the QSL landscape [19–29]. However, these efforts typically fix a single distinguishability measure at the outset, leaving open the question of whether a unified principle underlies all fidelity-based QSLs.

The notion of a "geometric approach" appears frequently in the QSL literature, yet its meaning can vary substantially depending on the context and the mathematical tools being employed. While it is often associated with fidelity-based distance measures, it can also refer to more rigorous constructions rooted in differential geometry and information geometry [15, 30–33].

An earlier and foundational example of geometric reasoning is due to Anandan and Aharonov [5], who derived a QSL for closed-system unitary evolution by considering the Fubini–Study distance between pure states. In this case, the speed limit arises naturally from the geometry of the projective Hilbert space and reflects the minimal time required for a quantum state to evolve into an orthogonal one [5].

In the work of Deffner and Lutz [15], the QSLs are framed in terms of the Bures angle, i.e., a functional of the Bures fidelity  $F_B(\rho_0, \rho_t)$  between the initial and final quantum states  $\rho_0$  and  $\rho_t$ , respectively [34–36]. Although their results are presented within a "geometric" perspective, no intrinsic metric properties of the Bures angle are used in the derivation. The essential role is played by the Bures fidelity  $F_B(\rho_0, \rho_t)$  itself, together with standard functional inequalities. In this sense, the approach is better understood as a *func*-

<sup>\*</sup> tristan.osan@unc.edu.ar

tional fidelity-based method, and not a genuinely geometric derivation in the information-geometric or Riemannian sense.

In contrast, Taddei et al. [18] developed a geometric QSL by directly using the quantum Fisher information, which defines a Riemannian metric on the space of quantum states. Their approach compares the length of the actual evolution path to the geodesic distance in this metric, making essential use of differential-geometric concepts. This method reveals that the speed limit arises not just from functional properties of fidelity, but from the underlying geometry of state space itself. While this formulation has a deep conceptual significance, its practical implementation becomes challenging when the initial state is mixed, as the QSL requires a minimization of the quantum Fisher information over all possible purifications in an enlarged system—environment Hilbert space.

This line of reasoning was extended by Pires et al. [32], who showed that many contractive Riemannian metrics—not just the Bures one—can generate valid QSLs. Their work demonstrates that one can construct an entire family of QSLs by choosing the appropriate metric structure, and that the tightest QSL may depend on the details of the physical dynamics.

From this landscape, it becomes clear that the phrase "geometric approach" can refer to rather different things: from a fidelity-based reformulation of dynamical bounds [15], to rigorous geometric derivations based on path length, metric contraction, and geodesics [18, 32].

One central objective of this work is to reexamine the assumptions underlying the geometric formulation as employed by Deffner and Lutz in their seminal work [15], as well as related approaches proposed in the literature (see, for example, Refs. [30, 31, 37]). This geometric viewpoint is based on the time derivative of a monotonic functional of a fidelitylike measure (e.g., the Bures angle in the case of the Bures fidelity). We show that this approach can be potentially misleading, as it may suggest that different monotonic functionals of a given fidelity measure could yield different QSLs. In contrast, we prove that any monotone and differentiable reparametrization of a selected fidelity yields identical ML/MT bounds, thereby rendering the QSL invariant under such transformations within this geometric approach and providing a unified perspective that connects fidelity- and metricinduced geometric formulations. Consequently, we show that the QSLs depend solely on the chosen generalized fidelity measure, rather than on any intrinsic metric structure associated with its functional form (e.g., the Bures angle). This observation motivates the generalized framework developed in the present work, which establishes a unified inequality structure valid for a broad class of distinguishability measures.

Within this theoretical framework, we also analyze several concrete QSLs derived from distinguishability measures between quantum states, commonly referred to as generalized fidelities or alternative fidelities—that is, measures conceptually similar to the well-known Bures fidelity but differing in definition and properties. These generalized fidelities are monotonic and differentiable functions that quantify the distinguishability between two quantum states and typically decrease as the states become more distinguishable. In general,

they satisfy some, but not necessarily all, of the properties of the Bures fidelity.

In addition, to explore the behavior of the QSLs analyzed in this work within a concrete physical setting, we consider the damped Jaynes–Cummings model, which describes the interaction between a two-level system and a single cavity mode that is, in turn, coupled to a reservoir composed of harmonic oscillators in the vacuum state.

This work is organized as follows. In Sec. II, we provide a brief overview of the Bures fidelity and its main properties. Sec. III introduces a set of alternative fidelity measures that fulfill a minimal set of desirable properties for quantifying the similarity between quantum states. In Sec. IV, we present our main analytical findings in the form of a proposition and a set of theorems. In Sec. V, we explore the behavior of the QSLs analyzed in this work within the physical setting provided by the damped Jaynes–Cummings model. Next, in Sec. VI, we analyze and discuss the analytical and numerical results obtained in this work. Finally, we introduce some concluding remarks in Sec. VII.

#### II. BURES FIDELITY

The Bures fidelity  $F_B$  (also known as the Uhlmann–Jozsa fidelity) is a widely used measure of the similarity between two density matrices. The Bures fidelity is defined as [34–36]

$$F_B(\rho, \sigma) = \left[ \text{Tr} \left( \sqrt{\sqrt{\rho} \, \sigma \, \sqrt{\rho}} \right) \right]^2,$$

where  $\rho$  and  $\sigma$  are arbitrary density matrices. The Bures fidelity  $F_B$  satisfies the four Jozsa axioms [36]:

(A1) Normalization:

$$0 \le F_B(\rho, \sigma) \le 1$$

(A2) Symmetry:

$$F_B(\rho, \sigma) = F_B(\sigma, \rho)$$

(A3) If  $\rho = |\psi\rangle\langle\psi|$  represents a pure state, then

$$F_B(\rho, \sigma) = \langle \psi | \sigma | \psi \rangle = \text{Tr}\{\rho \sigma\}$$

(A4) *Unitary invariance*: For any arbitrary unitary process  $\mathcal{U}, F_B(\rho, \sigma)$  is preserved i.e.,

$$F_B(\mathcal{U}\rho\mathcal{U}^{\dagger},\mathcal{U}\sigma\mathcal{U}^{\dagger}) = F_B(\rho,\sigma)$$

In addition to four Jozsa's axioms (A1)–(A4), the Bures fidelity  $F_B$  also satisfies the following properties [36, 38, 39]:

(P1) Identity of indiscernibles:

$$F_B(\rho,\sigma)=1$$
 if and only if  $\rho=\sigma$ 

(P2) Separate concavity: For  $p_1, p_2 \ge 0$ ,  $p_1 + p_2 = 1$ , and arbitrary density matrices  $\rho_1, \rho_2$  and  $\sigma$ 

$$F_B(p_1\rho_1 + p_2\rho_2, \sigma) \ge p_1F_B(\rho_1, \sigma) + p_2F_B(\rho_2, \sigma)$$

By symmetry property (A2), concavity in the second argument is also fulfilled.

(P3) Multiplicativity under tensor product: For arbitrary density matrices  $\rho_1$ ,  $\rho_2$ ,  $\sigma_1$  and  $\sigma_2$ 

$$F_B(\rho_1 \otimes \rho_2, \sigma_1 \otimes \sigma_2) = F_B(\rho_1, \sigma_1) F_B(\rho_2, \sigma_2)$$

(P4) *Monotonicity under quantum operations:* For a general quantum operation  $\mathcal{E}$  described by a completely positive trace-preserving map (CPTP-map),

$$F_B(\mathcal{E}(\rho), \mathcal{E}(\sigma)) \ge F_B(\rho, \sigma)$$

It is worth mentioning that  $F_B$  can be physically interpreted as a generalized transition probability between two mixed states  $\rho$  and  $\sigma$ . Some authors omit the square operation after performing the trace operation. In this case, the fidelity cannot be interpreted as a probability.

Generally speaking, the Bures fidelity can be difficult to compute. As a consequence, several alternative fidelity measures have been introduced in an effort to overcome this difficulty.

## III. ALTERNATIVE FIDELITY MEASURES

If one is willing to relax some of the properties of the Bures fidelity, a number of so-called generalized (or alternative) fidelities can be introduced. Below, we summarize several of these measures.

An upper bound of the Bures fidelity  $F_B$ , known as the *super-fidelity*  $\mathcal{F}_s$  [40, 41], is defined as follows:

$$\mathcal{F}_s(\rho,\sigma) = \text{Tr}\{\rho\sigma\} + \sqrt{1 - \text{Tr}\{\rho^2\}}\sqrt{1 - \text{Tr}\{\sigma^2\}}.$$
 (1)

It is worth noting that, in the particular case of qubits,  $\mathcal{F}_s$  coincides with the Bures fidelity  $F_B$ .

The super-fidelity  $\mathcal{F}_s(\rho, \sigma)$  defined by Eq. (1) satisfies all of Jozsa's axioms (A1)–(A4) [40, 41]. Additionally,  $\mathcal{F}_s$  is super-multiplicative under tensor products [40, 41], i.e.,

$$\mathcal{F}_s(\rho_1 \otimes \rho_2, \sigma_1 \otimes \sigma_2) \geq \mathcal{F}_s(\rho_1, \sigma_1) \mathcal{F}_s(\rho_2, \sigma_2).$$

The so-called operator fidelity is defined as follows [42]:

$$\mathcal{F}_o(\rho, \sigma) = \frac{\text{Tr}\{\rho\sigma\}}{\sqrt{\text{Tr}\{\rho^2\}}\sqrt{\text{Tr}\{\sigma^2\}}}.$$
 (2)

This quantity is often easier to compute than the Bures fidelity  $F_B$ . The operator fidelity  $\mathcal{F}_o(\rho,\sigma)$  defined by Eq. (2) satisfies Jozsa's axioms (A1), (A2), and (A4), as well as properties (P1) and (P3) [42].

If both the initial state  $\rho$  and the state  $\sigma$  represent pure states, it is straightforward to verify that the operator fidelity equals the Bures fidelity.

An alternative fidelity between quantum states was introduced in Ref. [43]:

$$\mathcal{F}_a(\rho, \sigma) = \left(1 + \sqrt{\frac{1 - \text{Tr}\{\rho^2\}}{\text{Tr}\{\rho^2\}}} \sqrt{\frac{1 - \text{Tr}\{\sigma^2\}}{\text{Tr}\{\sigma^2\}}}\right) \text{Tr}\{\rho\sigma\}.$$
(3)

In particular, if the initial state  $\rho_0$  represents a pure state, it is easy to see that this alternative fidelity equals the Bures fidelity.

The alternative fidelity  $\mathcal{F}_a$  satisfies all of Jozsa's axioms (A1)–(A4) and vanishes when the two density matrices are orthogonal [43]. Additionally,  $\mathcal{F}_a$  is super-multiplicative under tensor products [43], i.e.,

$$\mathcal{F}_a(\rho_1 \otimes \rho_2, \sigma_1 \otimes \sigma_2) \geq \mathcal{F}_a(\rho_1, \sigma_1) \mathcal{F}_a(\rho_2, \sigma_2).$$

#### IV. ANALYTICAL RESULTS

**Proposition 1.** Let D(x) be a bounded function defined on the domain [0,1], assumed to be continuous, monotonically decreasing, and differentiable. Furthermore, suppose that its inverse function  $D^{-1}(y)$  exists on the image of D and is also differentiable.

Consider the following functional composition:

$$\mathcal{L}_D(t) \doteq D\left(\mathcal{F}(\rho_0, \rho_t)\right) \equiv D(\mathcal{F}(t)),\tag{4}$$

where  $\mathcal{F}(\rho_0, \rho_t) \equiv \mathcal{F}(t)$  denotes a suitable measure of fidelity between an initial quantum state  $\rho_0$  and the evolved state  $\rho_t$  at time t. Under these assumptions, the following inequality holds:

$$-\frac{d}{dt}D^{-1}\left(\mathcal{L}_D(t)\right) \le \left|\dot{\mathcal{F}}(t)\right|. \tag{5}$$

Proof:

Let us consider the composite function  $\mathcal{L}_D(t) = D(\mathcal{F}(t))$ , where the function D(x) satisfies the properties stated in the proposition 1. Therefore, it follows that the general fidelity  $\mathcal{F}(t)$  can be expressed as  $\mathcal{F}(t) = D^{-1}(\mathcal{L}_D(t))$ . Now, we take the time derivative of Eq. (4):

$$\frac{d}{dt} \left( \mathcal{L}_D(\mathcal{F}(t)) \right) \le \left| \frac{d}{dt} \left( \mathcal{L}_D(\mathcal{F}(t)) \right) \right| = \left| \frac{d\mathcal{L}_D}{d\mathcal{F}} \right| \cdot \left| \dot{\mathcal{F}}(t) \right|.$$

Hence, we obtain:

$$\frac{d\mathcal{L}_D(t)}{dt} = \dot{\mathcal{L}}_D(t) = \frac{dD}{d\mathcal{F}} \cdot \frac{d\mathcal{F}(t)}{dt} \le \left| \frac{d\mathcal{L}_D(t)}{dt} \right| = \left| \frac{dD}{d\mathcal{F}} \right| \cdot \left| \frac{d\mathcal{F}(t)}{dt} \right|.$$

Given that D(x) is monotonically decreasing and differentiable, we have dD/dx < 0, implying that |dD/dx| = -dD/dx. Thus, the inequality simplifies to:

$$\dot{\mathcal{L}}_D(t) \le -\frac{dD}{d\mathcal{F}} \cdot \left| \frac{d\mathcal{F}(t)}{dt} \right|.$$

Next, we compute  $dD/d\mathcal{F}$  by differentiating the inverse function (note that this approach uses the inverse function theorem in reverse form):

$$\frac{dD}{d\mathcal{F}} = \left. \frac{1}{\frac{dD^{-1}(\mathcal{L}_D)}{d\mathcal{L}_D}} \right|_{\mathcal{L}_D = D(\mathcal{F})}.$$

Substituting this result into the previous inequality yields:

$$\dot{\mathcal{L}}_D(t) \le -\left(\frac{1}{\frac{dD^{-1}(\mathcal{L}_D)}{d\mathcal{L}_D}\bigg|_{\mathcal{L}_D = D(\mathcal{F})}}\right) \cdot \left|\frac{d\mathcal{F}(t)}{dt}\right|.$$

This inequality can be rewritten as:

$$-\frac{dD^{-1}(\mathcal{L}_D)}{d\mathcal{L}_D} \cdot \dot{\mathcal{L}}_D(t) \le \left| \dot{\mathcal{F}}(t) \right|.$$

Finally, taking into account the chain rule for differentiating the composition  $D^{-1}(\mathcal{L}_D(t))$ , we arrive at:

$$-\frac{dD^{-1}(\mathcal{L}_D(t))}{dt} \le \left| \dot{\mathcal{F}}(t) \right|,\,$$

which completes the proof of the proposition.

**Theorem 1.** Let D(x) be a function that satisfies the properties stated in Proposition 1.

Consider the following functional composition:

$$\mathcal{L}_D(t) \doteq D\left(\mathcal{F}(\rho_0, \rho_t)\right) \equiv D(\mathcal{F}(t)),\tag{6}$$

where  $\mathcal{F}(\rho_0, \rho_t) \equiv \mathcal{F}(t)$  denotes a suitable measure of fidelity between an initial quantum state  $\rho_0$  and the evolved state  $\rho_t$ at time t, such that  $0 \leq \mathcal{F}(t) \leq 1$ , with  $\mathcal{F}(0) = 1$ . Also, assume that there exists a function B(t) which upper bounds the absolute value of the time derivative of  $\mathcal{F}(t)$ , i.e.,

$$|\dot{\mathcal{F}}(t)| \le B(t), \quad \forall t \ge 0.$$

We define the time-averaged bound over the interval  $0 \le t \le \tau$  as

$$\mathcal{B}(\tau) \doteq \frac{1}{\tau} \int_0^{\tau} B(t) \, dt. \tag{7}$$

Then, the inequality

$$-\frac{dD^{-1}(\mathcal{L}_D(t))}{dt} \le |\dot{\mathcal{F}}(t)|$$

leads to the following QSL:

$$\tau_{QSL} \doteq \frac{1 - \mathcal{F}(\tau)}{\mathcal{B}(\tau)}.$$
(8)

The QSL expressed in Eq. (8) holds universally, irrespective of the specific choice of the function D(x), provided D(x) satisfies the properties stated in Proposition 1.

Proof:

We start from Eq. (5), i.e.,

$$-\frac{dD^{-1}(\mathcal{L}_D(t))}{dt} \le |\dot{\mathcal{F}}(t)|,$$

as  $|\dot{\mathcal{F}}(t)| \leq B(t)$  for  $t \geq 0$ , we can write

$$-\frac{dD^{-1}(\mathcal{L}_D(t))}{dt} \le B(t). \tag{9}$$

Integrating Eq. (9) over the time interval  $0 \le t \le \tau$  gives the following QSL:

$$au_{ extsf{QSL}} \doteq rac{[1-\mathcal{F}( au)]}{\mathcal{B}( au)},$$

where the quantity  $\mathcal{B}(\tau)$  is given by Eq. (7). These last results complete the proof.

**Corollary 1** (Immediate). Under the hypotheses of Theorem 1, all strictly monotone differentiable post-processing functionals  $g(\mathcal{F})$  generate the same QSL as using  $\mathcal{F}$  itself. Thus, within this geometric construction, no such reparametrization can produce a strictly tighter QSL.

To illustrate concrete examples derived from Proposition 1 and Theorem 1, we now introduce Theorems 2, 3, 4 and 5, which follow directly from these results when a specific form of the similarity measure between quantum states is chosen.

**Theorem 2.** Let D(x) be a function that satisfies the properties stated in Proposition 1. Also, define the following functional composition:

$$\mathcal{L}_D(t) \doteq D(F_B(\rho_0, \rho_t)) \equiv D(F_B(t)),$$

where  $F_B$  denotes the Bures fidelity (c.f. Sec. II) which depends on the initial and final quantum states  $\rho_0$  and  $\rho_t$ , respectively. Then, the following QSLs hold independently of the specific choice of the function D(x), provided D(x) satisfies the properties stated in Proposition 1:

• ML-type QSLs:

o Unitary (Hamiltonian) dynamics:

$$\tau_{QSL}^{B} \doteq \frac{\hbar}{2E_{\tau}} \left[ 1 - F_{B}(\tau) \right], \tag{10}$$

where  $E_{\tau}$  is the time-averaged energy defined by:

$$E_{\tau} \equiv \langle E \rangle_{\tau} = \frac{1}{\tau} \int_{0}^{\tau} \langle H_{t} \rangle \, \mathrm{d}t, \tag{11}$$

and  $\langle H_t \rangle \doteq \text{Tr}\{|H_t \rho(t)|\}.$ 

o Non-unitary evolution:

Consider now the case of a general nonunitary evolution described by the time-local master equation:

$$\dot{\rho}_t = L_t(\rho_t),$$

where  $L_t$  is the dynamics generator [44–46]. The QSL in this case is:

$$\tau_{QSL}^{B} \doteq \max \left\{ \frac{1}{\mathcal{B}^{(op)}(\tau)}, \frac{1}{\mathcal{B}^{(Tr)}(\tau)} \right\} \left[ 1 - F_{B}(\tau) \right],$$
(12)

where the quantities  $\mathcal{B}^{(op)}(\tau)$  and  $\mathcal{B}^{(Tr)}(\tau)$  are defined by:

$$\mathcal{B}^{(op)}(\tau) = \frac{1}{\tau} \int_0^{\tau} \|L_t(\rho_t)\|_{op} \, \mathrm{d}t, \tag{13}$$

$$\mathcal{B}^{(T_t)}(\tau) = \frac{1}{\tau} \int_0^{\tau} \|L_t(\rho_t)\|_{_{tr}} dt.$$
 (14)

# • MT-type QSL

The QSL in this case is:

$$\tau_{QSL}^{B} \doteq \frac{1}{\mathcal{B}^{(HS)}(\tau)} \left[ 1 - F_B(\tau) \right], \tag{15}$$

where

$$\mathcal{B}^{(HS)}(\tau) = \frac{1}{\tau} \int_0^{\tau} dt \ \|L_t(\rho_t)\|_{HS}, \tag{16}$$

and the Hilbert–Schmidt norm is defined, for a given operator A, as

$$\|A\|_{_{H\!S}} = \sqrt{ ext{Tr}\{A^\dagger A\}} = \sqrt{\sum_i \sigma_i^2},$$

where  $\{\sigma_i\}$  are the singular values of A [47].

Proof:

• ML-type QSLs

# o Hamiltonian Dynamics:

Consider a quantum system evolving under a time-dependent Hamiltonian  $H_t$ . The time evolution of the system's density operator  $\rho_t$  is governed by the von Neumann's equation:

$$\dot{\rho}_t = \frac{1}{i\hbar} \left[ H_t, \rho_t \right]. \tag{17}$$

Assuming the system starts in a pure state  $\rho_0 = |\psi_0\rangle\langle\psi_0|$ , Eq. (5) in proposition (1) becomes

$$-\frac{dD^{-1}(\mathcal{L}_D(t))}{dt} \le |\langle \psi_0 | \, \dot{\rho}_t \, | \psi_0 \rangle| \,. \tag{18}$$

Substituting Eq. (17) into Eq. (18), we obtain:

$$-\frac{dD^{-1}(\mathcal{L}_D(t))}{dt} \leq \frac{1}{\hbar} \left| \langle \psi_0 | [H_t, \rho_t] | \psi_0 \rangle \right|.$$

Applying the triangle inequality to the right-hand side, we arrive at:

$$-\frac{dD^{-1}(\mathcal{L}_D(t))}{dt} \le \frac{1}{\hbar} \left( |\operatorname{Tr}\{H_t \rho_t \rho_0\}| + |\operatorname{Tr}\{\rho_t H_t \rho_0\}| \right).$$

To estimate an upper bound for the terms on the right-hand side, we use the von Neumann's trace inequality [15, 48–50]. Taking  $A = (H_t \rho_t)^{\dagger} = \rho_t H_t$  and applying von Neumann's trace inequality [15, 48–50], we find:

$$-\frac{dD^{-1}(\mathcal{L}_D(t))}{dt} \le \frac{2}{\hbar} \sum_i \sigma_i p_i = \frac{2}{\hbar} \sigma_1,$$

where  $\sigma_i$  are the singular values of  $H_t \rho_t$  (with  $\sigma_1 \geq \sigma_2 \geq \cdots \geq \sigma_n$ ), and  $p_i = \delta_{i,1}$  follows from the pure initial state  $\rho_0$ . For Hermitian operators, the operator norm equals the largest singular value, i.e.,  $||A||_{\rm op} = \sigma_1$ , while the trace norm equals the sum of all singular values, i.e.,  $||A||_{\rm Tr} = \sum_i \sigma_i$  [47]. Hence,

$$-\frac{dD^{-1}(\mathcal{L}_{D}(t))}{dt} \le \frac{2}{\hbar} \|H_{t}\rho_{t}\|_{\text{op}} \le \frac{2}{\hbar} \|H_{t}\rho_{t}\|_{\text{Tr}}.$$
 (19)

If the instantaneous eigenvalues of  $H_t$  are positive (which can always be ensured by an appropriate choice of the energy zero [2]), the trace norm becomes:

$$||H_t \rho_t||_{\operatorname{Tr}} = \operatorname{Tr}\{|H_t \rho_t|\} = \langle H_t \rangle.$$

Thus, equation (19) can be written as:

$$-\frac{dD^{-1}(\mathcal{L}_D(t))}{dt} \le \langle H_t \rangle. \tag{20}$$

Integrating Eq. (20) over the time interval  $0 \le t \le \tau$  yields

$$au_{ ext{QSL}}^{B} \doteq rac{\hbar}{2E} \left[ 1 - F_{B}( au) 
ight],$$

where  $E_{\tau}$  is given by Eq. (11).

• Non-Unitary Evolution:

Now consider an arbitrary time-dependent nonunitary evolution governed by

$$\dot{\rho}_t = L_t(\rho_t),\tag{21}$$

where  $L_t$  is the dynamics generator [44–46]. These generators are trace-class superoperators in a complex Banach space and may be non-Hermitian. However, for symmetric norms such as the Schatten p-norm,  $||L_t||_p = (\sum_i \lambda_i^p)^{1/p}$  [51], the equality  $||L_t^{\dagger}|| = ||L_t||$  holds, ensuring the validity of previous equations and bounds [15, 52].

Substituting Eq. (21) into Eq. (18) yields:

$$-\frac{dD^{-1}(\mathcal{L}_D(t))}{dt} \le \left| \left\langle \psi_0 \right| L_t(\rho_t) \left| \psi_0 \right\rangle \right| = \left| \text{Tr} \left\{ L_t(\rho_t) \rho_0 \right\} \right|.$$

Applying the von Neumann's trace inequality [15, 48–50] again, we obtain

$$-\frac{dD^{-1}(\mathcal{L}_D(t))}{dt} \le \sum_i \lambda_i p_i = \lambda_1, \tag{22}$$

where  $\lambda_i$  (with  $\lambda_1 \geq \lambda_2 \geq \cdots \geq \lambda_n$ ) are the singular values of  $L_t(\rho_t)$ . Using the norm hierarchy, we further bound Eq. (22):

$$-\frac{dD^{-1}(\mathcal{L}_D(t))}{dt} \le \|L_t(\rho_t)\|_{\text{op}} \le \|L_t(\rho_t)\|_{\text{Tr}}.$$
 (23)

In analogy with Ref. [15], integrating Eq. (23) over the time interval  $0 \le t \le \tau$  allows us to obtain a ML-type QSL for open quantum systems as follows

$$au_{ ext{QSL}}^{B} \doteq \max \left\{ rac{1}{\mathcal{B}_{ au}^{( ext{cop})}}, rac{1}{\mathcal{B}_{ au}^{( ext{Tr})}} 
ight\} \left[ 1 - F_{B}( au) 
ight],$$

where  $\mathcal{B}^{\text{(op)}}(\tau)$  and  $\mathcal{B}^{\text{(Tr)}}(\tau)$  are given by Eqs. (13) and (14).

• MT-type OSL

To derive a MT-type QSL in the case of arbitrary positive open-system dynamics, we follow refs. [16] and [15].

Substituting Eq. (21) into Eq. (18) yields:

$$-\frac{dD^{-1}(\mathcal{L}_D(t))}{dt} \le |\operatorname{Tr}\{L_t(\rho_t)\rho_0\}|.$$

Applying the Cauchy–Schwarz inequality for operators [15, 16] we obtain:

$$-\frac{dD^{-1}(\mathcal{L}_D(t))}{dt} \le \sqrt{\text{Tr}\{L_t(\rho_t)L_t(\rho_t)^{\dagger}\} \text{Tr}\{\rho_0^2\}}.$$

For a pure initial state  $\rho_0$ ,  $\text{Tr}\{\rho_0^2\} = 1$ , hence:

$$-\frac{dD^{-1}(\mathcal{L}_D(t))}{dt} \le \sqrt{\text{Tr}\{L_t(\rho_t)L_t(\rho_t)^{\dagger}\}} = \|L_t(\rho_t)\|_{\text{HS}},$$
(24)

where the Hilbert-Schmidt norm is defined as  $||A||_{HS}$  $\sqrt{\text{Tr}\{A^{\dagger}A\}} = \sqrt{\sum_{i} \sigma_{i}^{2}}$  [47]. Integrating Eq. (24) over the time interval  $0 \le t \le \tau$  gives the following QSL:

$$au_{ ext{QSL}}^{B} \doteq rac{\left[1 - F_{B}( au)
ight]}{\mathcal{B}^{ ext{(HS)}}( au)},$$

where the quantity  $\mathcal{B}^{\text{(HS)}}(\tau)$  is given by Eq. (16). These last results complete the proof. 

**Theorem 3.** Let D(x) be a function that satisfies the properties stated in Proposition 1. Also, define the following functional composition:

$$\mathcal{L}_D(t) \doteq D(\mathcal{F}_s(\rho_0, \rho_t)) \equiv D(\mathcal{F}_s(t)),$$

where  $\mathcal{F}_s(t)$  denotes the super-fidelity given by

$$\mathcal{F}_s(t) = \text{Tr}\{\rho_0 \rho_t\} + \sqrt{1 - \text{Tr}\{\rho_0^2\}} \sqrt{1 - \text{Tr}\{\rho_t^2\}}.$$

(cf. Eq. (1)), Sec. III), which depends on the initial and final quantum states  $\rho_0$  and  $\rho_t$ , respectively. Consider the case of a general nonunitary evolution described by the time-local master equation:

$$\dot{\rho}_t = L_t(\rho_t),$$

where  $L_t$  is the dynamics generator [44–46]. Then, the following QSLs hold independently of the specific choice of the function D(x), provided D(x) satisfies the properties stated in Proposition 1:

• ML-type QSLs:

The QSL in this case is:

$$\tau_{QSL}^{s} \doteq \max \left\{ \frac{1}{\mathcal{B}_{s}^{(op)}(\tau)}, \frac{1}{\mathcal{B}_{s}^{(Tr)}(\tau)} \right\} \left[ 1 - \mathcal{F}_{s}(\tau) \right], \tag{25}$$

where the quantities  $\mathcal{B}_{s}^{(op)}(\tau)$  and  $\mathcal{B}_{s}^{(Tr)}(\tau)$  are given by

$$\mathcal{B}_{s}^{(op)}(\tau) \doteq \frac{1}{\tau} \int_{0}^{\tau} |\|L_{t}(\rho_{t})|\|_{op} \cdot \left(1 + \sqrt{\frac{1 - \text{Tr}\{\rho_{0}^{2}\}}{1 - \text{Tr}\{\rho_{t}^{2}\}}}\right) dt,$$
(26)

$$\mathcal{B}_{s}^{(T_{t})}(\tau) \doteq \frac{1}{\tau} \int_{0}^{\tau} \left| \left| L_{t}(\rho_{t}) \right| \right|_{\tau} \cdot \left( 1 + \sqrt{\frac{1 - \text{Tr}\{\rho_{0}^{2}\}}{1 - \text{Tr}\{\rho_{t}^{2}\}}} \right) dt.$$
(27)

• MT-type QSL:

The QSL in this case is:

$$\tau_{QSL}^{s} = \frac{\left[1 - \mathcal{F}_{s}(\tau)\right]}{\mathcal{B}_{s}^{(HS)}(\tau)},\tag{28}$$

where

$$\mathcal{B}_s^{(HS)}(\tau) = \frac{1}{\tau} \int_0^{\tau} dt \, \|L_t(\rho_t)\|_{HS} \cdot \left(1 + \sqrt{\frac{1 - \text{Tr}\{\rho_0^2\}}{1 - \text{Tr}\{\rho_t^2\}}}\right). \tag{29}$$

Proof:

We start from Eq. (5), i.e.,

$$-\frac{d}{dt}D^{-1}\left(\mathcal{L}_D(t)\right) \le \left|\dot{\mathcal{F}}_s(t)\right|,\tag{30}$$

and, bearing in mind Ref. [37], we notice that the absolute value of the time derivative of the super-fidelity  $\mathcal{F}_s(\rho_0, \rho_t)$  is given by

$$\left| \dot{\mathcal{F}}_{s}(t) \right| = \left| \text{Tr} \{ \rho_{0} \dot{\rho}_{t} \} - \sqrt{\frac{1 - \text{Tr} \{ \rho_{0}^{2} \}}{1 - \text{Tr} \{ \rho_{t}^{2} \}}} \, \text{Tr} \{ \rho_{t} \dot{\rho}_{t} \} \right| 
\leq \left| \text{Tr} \{ \rho_{0} \dot{\rho}_{t} \} \right| + \sqrt{\frac{1 - \text{Tr} \{ \rho_{0}^{2} \}}{1 - \text{Tr} \{ \rho_{t}^{2} \}}} \, \left| \text{Tr} \{ \rho_{t} \dot{\rho}_{t} \} \right|.$$
(31)

For general non-unitary dynamics, the evolution of the density operator is governed by a time-local master equation of the form  $\dot{\rho}_t = L_t(\rho_t)$ . Substituting (31) into Eq. (30), we obtain:

$$-\frac{dD^{-1}(\mathcal{L}_{D}(t))}{dt} \leq |\text{Tr}\{\rho_{0}L_{t}(\rho_{t})\}| + \sqrt{\frac{1 - \text{Tr}\{\rho_{0}^{2}\}}{1 - \text{Tr}\{\rho_{t}^{2}\}}} |\text{Tr}\{\rho_{t}L_{t}(\rho_{t})\}|. \quad (32)$$

#### • ML-type QSLs

Applying von Neumann's trace inequality [15, 48–50] to the first term on the right-hand side of Eq. (32), we obtain

$$|\text{Tr}\{\rho_0 L_t(\rho_t)\}| \leqslant \sum_i p_i \lambda_i,$$

where  $\{p_i\}$  (with  $p_1 \geq p_2 \geq \cdots \geq p_n$ ) and  $\lambda_i$  (with  $\lambda_1 \geq \lambda_2 \geq \cdots \geq \lambda_n$ ) are the singular values of  $\rho_0$  and  $L_t(\rho_t)$ , respectively. Similarly, for the second term:

$$|\text{Tr}\{\rho_t L_t(\rho_t)\}| \leqslant \sum_i \epsilon_i \lambda_i,$$

where  $\{\epsilon_i\}$  (with  $\epsilon_1 \geq \epsilon_2 \geq \cdots \geq \epsilon_n$ ) are the singular values of  $\rho_t$ .

Since  $p_i \leq 1$  and  $\epsilon_i \leq 1$ , it follows that

$$\sum_{i} p_i \lambda_i \le \lambda_1 \le \sum_{i} \lambda_i, \qquad \sum_{i} \epsilon_i \lambda_i \le \lambda_1 \le \sum_{i} \lambda_i,$$

where  $\lambda_1$  is the largest singular value of  $L_t(\rho_t)$ , which corresponds to the operator norm  $\|L_t(\rho_t)\|_{\text{op}}$ , while the sum  $\sum_i \lambda_i$  gives the trace norm  $\|L_t(\rho_t)\|_{\text{Tr}}$ . Thus, we can write

$$-\frac{dD^{-1}(\mathcal{L}_{D}(t))}{dt} \leqslant ||L_{t}(\rho_{t})||_{_{\text{op,Tr}}} \left(1 + \sqrt{\frac{1 - \text{Tr}\{\rho_{0}^{2}\}}{1 - \text{Tr}\{\rho_{t}^{2}\}}}\right)$$
(33)

In analogy with Ref. [15], integrating Eq. (33) over the time interval  $0 \le t \le \tau$  allows us to obtain a ML-type QSL for open quantum systems as follows

$$au_{ extsf{QSL}}^{s} = \max \left\{ rac{1}{\mathcal{B}_{s}^{( ext{op})}( au)}, rac{1}{\mathcal{B}_{s}^{( ext{Tr})}( au)} 
ight\} \left[ 1 - \mathcal{F}_{s}( au) 
ight],$$

where the time-averaged quantities  $\mathcal{B}_{s}^{\text{(op)}}(\tau)$  and  $\mathcal{B}_{s}^{\text{(Tr)}}(\tau)$  are given by Eqs. (26) and (27).

#### • MT-type QSL

Using the Cauchy–Schwarz inequality for operators [15, 16], we can bound Eq. (32) in the following way:

$$-\frac{dD^{-1}(\mathcal{L}_{D}(t))}{dt} \leq \sqrt{\operatorname{Tr}\{\rho_{0}^{2}\}} \sqrt{\operatorname{Tr}\left\{L_{t}^{\dagger}(\rho_{t})L_{t}(\rho_{t})\right\}} + \sqrt{\frac{1 - \operatorname{Tr}\{\rho_{0}^{2}\}}{1 - \operatorname{Tr}\{\rho_{t}^{2}\}}} \sqrt{\operatorname{Tr}\{\rho_{t}^{2}\}} \sqrt{\operatorname{Tr}\left\{L_{t}^{\dagger}(\rho_{t})L_{t}(\rho_{t})\right\}}$$

$$\leq \left(1 + \sqrt{\frac{1 - \operatorname{Tr}\{\rho_{0}^{2}\}}{1 - \operatorname{Tr}\{\rho_{t}^{2}\}}}\right) \|L_{t}(\rho_{t})\|_{\operatorname{HS}},$$

$$(34)$$

where the last step uses the fact that  $\mathrm{Tr}\big\{\rho^2\big\} \leq 1$  for any density operator, and  $\|L_t(\rho_t)\|_{\mathrm{HS}} = \sqrt{\sum_i \lambda_i^2}$  denotes the Hilbert–Schmidt norm of  $L_t(\rho_t)$ .

Integrating Eq. (34) over the time interval  $0 \le t \le \tau$  gives the following MT-type QSL for non-unitary evolution:

$$au_{ ext{QSL}}^{s} \doteq rac{\left[1 - \mathcal{F}_{s}( au)
ight]}{\mathcal{B}_{s}^{ ext{(HS)}}( au)},$$

where  $\mathcal{B}_s^{\text{(HS)}}(\tau)$  is given by Eq. (29)

These last results complete the proof.  $\Box$ 

**Theorem 4.** Let D(x) be a function that satisfies the properties stated in Proposition 1. Also, define the following functional composition:

$$\mathcal{L}_D(t) \doteq D(\mathcal{F}_o(\rho_0, \rho_t)) \equiv D(\mathcal{F}_o(t)), \tag{35}$$

where  $\mathcal{F}_o(t)$  denotes the operator fidelity given by

$$\mathcal{F}_o(t) = \frac{\left| \operatorname{Tr} \{ \rho_0 \rho_t \} \right|}{\sqrt{\operatorname{Tr} \{ \rho_0^2 \}} \sqrt{\operatorname{Tr} \{ \rho_t^2 \}}},$$

(cf. Eq. (2)), Sec. III, which depends on the initial and final quantum states  $\rho_0$  and  $\rho_t$ , respectively. Consider the case of a general nonunitary evolution described by the time-local master equation:

$$\dot{\rho}_t = L_t(\rho_t),$$

where  $L_t$  is the dynamics generator [44–46]. Then, the following MT-type QSL holds independently of the specific choice of the function D(x), provided D(x) satisfies the properties stated in Proposition 1:

$$\tau_{\scriptscriptstyle QSL}^{o} \doteq \frac{1 - \mathcal{F}_{o}(\tau)}{\mathcal{B}_{o}(\tau)},\tag{36}$$

where the quantity  $\mathcal{B}_o(\tau)$  is given by the following equation:

$$\mathcal{B}_o(\tau) \doteq \frac{2}{\tau} \int_0^{\tau} \sqrt{\frac{\text{Tr}\{\dot{\rho}_t^2\}}{\text{Tr}\{\rho_t^2\}}} dt$$
 (37)

Proof:

We start from Eq. (5), i.e.,

$$-\frac{d}{dt}D^{-1}\left(\mathcal{L}_D(t)\right) \le \left|\dot{\mathcal{F}}_o(t)\right|,\,$$

and, bearing in mind Ref. [53], we notice that the absolute value of the time derivative of the operator fidelity  $\mathcal{F}_o(t)$  is given by

$$\left| \dot{\mathcal{F}}_o(t) \right| = \left| \frac{\operatorname{Tr}\{\rho_0 \dot{\rho}_t\}}{\sqrt{\operatorname{Tr}\{\rho_0^2\}} \sqrt{\operatorname{Tr}\{\rho_t^2\}}} - \frac{\operatorname{Tr}\{\rho_0 \rho_t\} \operatorname{Tr}\{\rho_t \dot{\rho}_t\}}{\sqrt{\operatorname{Tr}\{\rho_0^2\}} \left[\operatorname{Tr}\{\rho_t^2\}\right]^{3/2}} \right|$$

Applying the triangle inequality to the right-hand side, we obtain:

$$\left| \dot{\mathcal{F}}_{o}(t) \right| \leq \frac{\left| \operatorname{Tr} \{ \rho_{0} \dot{\rho}_{t} \} \right|}{\sqrt{\operatorname{Tr} \{ \rho_{o}^{2} \}} \sqrt{\operatorname{Tr} \{ \rho_{t}^{2} \}}} + \frac{\left| \operatorname{Tr} \{ \rho_{0} \rho_{t} \} \operatorname{Tr} \{ \rho_{t} \dot{\rho}_{t} \} \right|}{\sqrt{\operatorname{Tr} \{ \rho_{0}^{2} \}} \left[ \operatorname{Tr} \{ \rho_{t}^{2} \} \right]^{3/2}}$$
(38)

Now, using the Cauchy–Schwarz inequality for operators [15, 16] on the right side of Eq. (38), we can write:

$$-\frac{d}{dt}D^{-1}\left(\mathcal{L}_D(t)\right) \le 2\sqrt{\frac{\operatorname{Tr}\{\dot{\rho}_t^2\}}{\operatorname{Tr}\{\rho_t^2\}}}$$
(39)

Integrating Eq. (39) over the time interval  $0 \le t \le \tau$  allows us to obtain a QSL as follows:

$$\tau_{\text{QSL}}^{o} \doteq \frac{1 - \mathcal{F}_{o}(\tau)}{\mathcal{B}_{o}(\tau)},\tag{40}$$

where the quantity  $\mathcal{B}_{o}(\tau)$  is given by (37).

These last results complete the proof.

**Theorem 5.** Let D(x) be a function that satisfies the properties stated in Proposition 1. Also, define the following functional composition:

$$\mathcal{L}_D(t) \doteq D(\mathcal{F}_a(\rho_0, \rho_t)) \equiv D(\mathcal{F}_a(t)),$$

where  $\mathcal{F}_a(t)$  denotes the alternative fidelity given by

$$\mathcal{F}_a(t) = \left(1 + \sqrt{\frac{1 - \text{Tr}\{\rho_0^2\}}{\text{Tr}\{\rho_0^2\}}} \sqrt{\frac{1 - \text{Tr}\{\rho_t^2\}}{\text{Tr}\{\rho_t^2\}}}\right) \text{Tr}\{\rho_0 \rho_t\},$$

(cf. Eq. (3)), Sec. III), which depends on the initial and final quantum states  $\rho_0$  and  $\rho_t$ , respectively. Consider the case of a general nonunitary evolution described by the time-local master equation:

$$\dot{\rho}_t = L_t(\rho_t),$$

where  $L_t$  is the dynamics generator [44–46]. Then, the following MT-type QSL holds independently of the specific choice of the function D(x), provided D(x) satisfies the properties stated in Proposition 1:

$$au_{ ilde{ extit{QSL}}}^a \doteq rac{1 - \mathcal{F}_a( au)}{\mathcal{B}_a( au)},$$

where the quantity  $\mathcal{B}_a(\tau)$  is given by the following equation:

$$\mathcal{B}_{a}(\tau) \doteq \frac{1}{\tau} \int_{0}^{\tau} \left( \sqrt{\frac{1 - \text{Tr}\{\rho_{0}^{2}\}}{\text{Tr}\{\rho_{0}^{2}\}}} \sqrt{\frac{\text{Tr}\{\rho_{t}^{2}\}}{1 - \text{Tr}\{\rho_{t}^{2}\}}} \left| \frac{\text{Tr}\{\dot{\rho}_{t}\rho_{t}\} \, \text{Tr}\{\rho_{0}\rho_{t}\}}{(\text{Tr}\{\rho_{t}^{2}\})^{2}} \right| + \sqrt{\text{Tr}\{\rho_{0}^{2}\} \, \text{Tr}\{\dot{\rho}_{t}^{2}\}} + \sqrt{\frac{1 - \text{Tr}\{\rho_{t}^{2}\}}{\text{Tr}\{\rho_{t}^{2}\}}} \sqrt{1 - \text{Tr}\{\rho_{0}^{2}\}} \sqrt{\text{Tr}\{\dot{\rho}_{t}^{2}\}} \right) dt.$$

$$(41)$$

Proof:

We start from Eq. (5), i.e.,

$$-\frac{d}{dt}D^{-1}\left(\mathcal{L}_D(t)\right) \le \left|\dot{\mathcal{F}}_a(t)\right|,\,$$

and, bearing in mind Ref. [43], we notice that the absolute value of the time derivative of the alternative fidelity  $\mathcal{F}_a(t)$  is given by

$$\left| \frac{d\mathcal{F}_a(t)}{dt} \right| = \left| \frac{-\operatorname{Tr}\{\dot{\rho_t}\rho_t\}}{(\operatorname{Tr}\{\rho_t\})^2} \sqrt{\frac{1-\operatorname{Tr}\{\rho_0^2\}}{\operatorname{Tr}\{\rho_0^2\}}} \sqrt{\frac{\operatorname{Tr}\{\rho_t^2\}}{1-\operatorname{Tr}\{\rho_t^2\}}} \operatorname{Tr}\{\rho_0\rho_t\} + \left(1+\sqrt{\frac{1-\operatorname{Tr}\{\rho_0^2\}}{\operatorname{Tr}\{\rho_0^2\}}} \sqrt{\frac{1-\operatorname{Tr}\{\rho_t^2\}}{\operatorname{Tr}\{\rho_t^2\}}}\right) \operatorname{Tr}\{\rho_0\dot{\rho_t}\} \right|.$$

Applying the triangle inequality we can write

$$\left| \frac{d\mathcal{F}_a(t)}{dt} \right| \leq \sqrt{\frac{1 - \text{Tr}\{\rho_0^2\}}{\text{Tr}\{\rho_0^2\}}} \sqrt{\frac{\text{Tr}\{\rho_t^2\}}{1 - \text{Tr}\{\rho_t^2\}}} \left| \frac{\text{Tr}\{\dot{\rho}_t \rho_t\} \, \text{Tr}\{\rho_0 \rho_t\}}{(\text{Tr}\{\rho_t\})^2} \right| + \left(1 + \sqrt{\frac{1 - \text{Tr}\{\rho_0^2\}}{\text{Tr}\{\rho_0^2\}}} \sqrt{\frac{1 - \text{Tr}\{\rho_t^2\}}{\text{Tr}\{\rho_t^2\}}} \right) |\text{Tr}\{\rho_0 \dot{\rho}_t\}|. \tag{42}$$

Thus, by using Cauchy-Schwarz inequality [15, 16] on the

second term of Eq. (42), we obtain:

$$-\frac{d}{dt}D^{-1}\left(\mathcal{L}_{D}(t)\right) \leq \sqrt{\frac{1 - \text{Tr}\{\rho_{0}^{2}\}}{\text{Tr}\{\rho_{0}^{2}\}}} \sqrt{\frac{\text{Tr}\{\rho_{t}^{2}\}}{1 - \text{Tr}\{\rho_{t}^{2}\}}} \left| \frac{\text{Tr}\{\dot{\rho}_{t}\rho_{t}\} \, \text{Tr}\{\rho_{0}\rho_{t}\}}{(\text{Tr}\{\rho_{t}\})^{2}} \right| + \sqrt{\text{Tr}\{\rho_{0}^{2}\} \, \text{Tr}\{\dot{\rho}_{t}^{2}\}} + \sqrt{\frac{1 - \text{Tr}\{\rho_{t}^{2}\}}{\text{Tr}\{\rho_{t}^{2}\}}} \sqrt{1 - \text{Tr}\{\dot{\rho}_{0}^{2}\}} \sqrt{\text{Tr}\{\dot{\rho}_{t}^{2}\}}.$$

$$(43)$$

Integrating Eq. (43) over the time interval  $0 \le t \le \tau$  allows us to obtain a QSL as follows

$$au_{ ext{QSL}}^{a} \doteq rac{1 - \mathcal{F}_{a}( au)}{\mathcal{B}_{a}( au)},$$

where the quantity  $\mathcal{B}_a(\tau)$  is given by Eq. (41). These last results complete the proof.

#### V. QUANTUM SPEED LIMITS IN A PHYSICAL MODEL

To analyze the behavior of the QSLs in a concrete physical setting, we shall consider the damped Jaynes–Cummings model, which admits an exact solution. This model describes the interaction between a two-level system and a single cavity mode, which in turn is coupled to a reservoir composed of harmonic oscillators in the vacuum state. When we restrict the dynamics to the single-excitation subspace of the system–cavity composite, the cavity mode can be eliminated by means of an effective spectral density of the form [46, 54]

$$J(\omega) = \frac{1}{2\pi} \frac{\gamma_0 \lambda^2}{(\omega_0 - \omega)^2 + \lambda^2},$$

where  $\omega_0$  denotes the transition frequency of the two-level system. The parameter  $\lambda$  characterizes the spectral width of the coupling and is related to the reservoir correlation time  $\tau_R$  through  $\tau_R = \lambda^{-1}$ . The characteristic time scale over which the state of the system evolves is given by  $\tau_S = \gamma_0^{-1}$ . In this model, the nonunitary generator of the reduced dynamics of the system is given by

$$L_t(\rho_t) = \gamma_t \left( \sigma_- \rho_t \sigma_+ - \frac{1}{2} \sigma_+ \sigma_- \rho_t - \frac{1}{2} \rho_t \sigma_+ \sigma_- \right), (44)$$

where  $\sigma_{\pm} = \sigma_x \pm i\sigma_y$  are the Pauli operators and  $\gamma_t$  is the time-dependent decay rate given by,

$$\gamma_t = \frac{2\gamma_0 \lambda \sinh(h_1 t/2)}{h_1 \cosh(h_1 t/2) + \lambda \sinh(h_1 t/2)},$$
 (45)

where  $h_1 = \sqrt{\lambda^2 - 2\gamma_0\lambda}$ .

The Bloch representation of a mixed initial quantum state (with a computational basis order  $\{|0\rangle\,, |1\rangle\}$ ) can be expressed

$$\rho_0 = \begin{pmatrix} 1 - \rho_{11}(0) & \rho_{01}(0) \\ \rho_{01}^*(0) & \rho_{11}(0) \end{pmatrix} = \frac{1}{2} \begin{pmatrix} 1 + r_z & r_x - ir_y \\ r_x + ir_y & 1 - r_z \end{pmatrix}, \tag{46}$$

where,  $r_x, r_y, r_z$  are the components of the Bloch vector.

The state of the quantum system at time t in this model is analytically given by [46, 54]

$$\rho_t = \begin{pmatrix} 1 - \rho_{11}(0)|q_t|^2 & \rho_{01}(0)q_t \\ \rho_{10}(0)q_t^* & \rho_{11}(0)|q_t|^2 \end{pmatrix}$$
(47)

where

$$q_{t} = e^{-\lambda t/2} \times \begin{cases} \cosh\left(\frac{h_{1}t}{2}\right) + \frac{\lambda}{h_{1}} \sinh\left(\frac{h_{1}t}{2}\right), & (\gamma_{0} \leq \lambda/2), \\ \cos\left(\frac{h_{2}t}{2}\right) + \frac{\lambda}{h_{2}} \sin\left(\frac{h_{2}t}{2}\right), & (\gamma_{0} > \lambda/2), \end{cases}$$

$$(48)$$

with  $h_2 = \sqrt{2\gamma_0\lambda - \lambda^2}$ .

The time derivative of the density matrix  $\rho_t$  can be written as:

$$\dot{\rho_t} = \begin{pmatrix} -2\rho_{11}(0)q_t\dot{q}_t & \rho_{01}(0)\dot{q}_t\\ \rho_{10}(0)\dot{q}_t & 2\rho_{11}(0)q_t\dot{q}_t \end{pmatrix}$$
(49)

Because  $\dot{p}_t$  is Hermitian (off-diagonal entries are conjugates and diagonal entries are real), its *singular values* are the *absolute values of its eigenvalues*. In this case, both singular values turn out to be equal and given by:

$$s_1 = s_2 = |\dot{q}_t| \sqrt{(2\rho_{11}(0)q_t)^2 + |\rho_{01}(0)|^2}.$$

The operator (spectral) norm is the *largest singular value*, thus, in terms of the components of the Bloch vector of the initial state  $\rho_0$  we can write:

$$\|\dot{\rho}_t\|_{\text{op}} = \frac{|\dot{q}_t|}{2} \sqrt{r_x^2 + r_y^2 + 4(1 - r_z)^2 q_t^2}.$$
 (50)

As the trace norm is the sum of singular values we have  $\|\dot{\rho}_t\|_1=2s_1$ . Furthermore, Hilbert–Schmidt norm  $\|\dot{\rho}_t\|_2=\sqrt{\mathrm{Tr}\Big\{\dot{\rho}_t^\dagger\dot{\rho}_t\Big\}}=\sqrt{s_1^2+s_2^2}=\sqrt{2}\,s_1$ . Thus, these three norms are all proportional to the same geometric factor  $\sqrt{r_x^2+r_y^2+4(1-r_z)^2q_t^2}$ , and we have:  $\|\dot{\rho}_t\|_1=2\|\dot{\rho}_t\|_{\mathrm{op}}$ , and  $\|\dot{\rho}_t\|_2=\sqrt{2}\|\dot{\rho}_t\|_{\mathrm{op}}$ 

#### A. Bures fidelity

Bearing in mind Ref. [15] we shall examine the case where the system is initially in the excited state, i.e.,  $\rho_0 = |1\rangle\langle 1|$ . In this case, from equations (12), (15), (46), and (47) we can write

$$\tau_{\text{QSL}}^{B} = \frac{1 - |q_{\tau}|^{2}}{\frac{2\mu}{\tau} \int_{0}^{\tau} dt \, |q_{t}| |\dot{q}_{t}|},\tag{51}$$

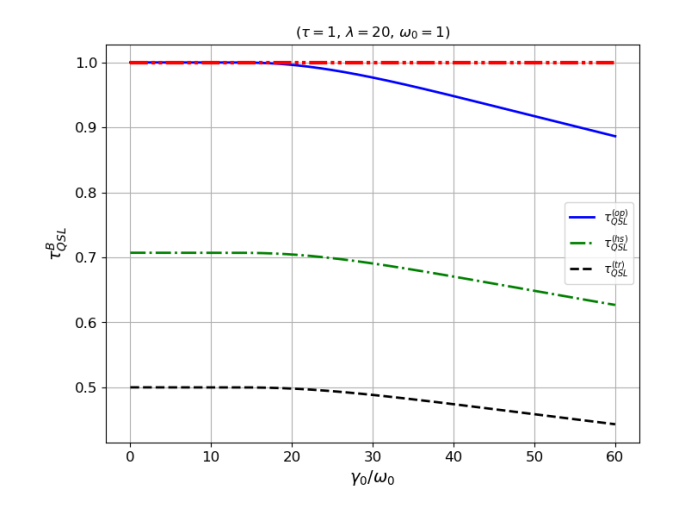


Figure 1. ML and MT QSLs  $au_{\rm QSL}^B$  given by Eq. (51), as a function of  $\gamma_0/\omega_0$  for the excited initial state given by  $\rho_0=|1\rangle\langle 1|$ . The evolution time was set as  $\tau=1,\lambda=20$ , and  $\omega_0=1$ . The horizontal dashed line represents the actual driving time  $\tau=1$ .

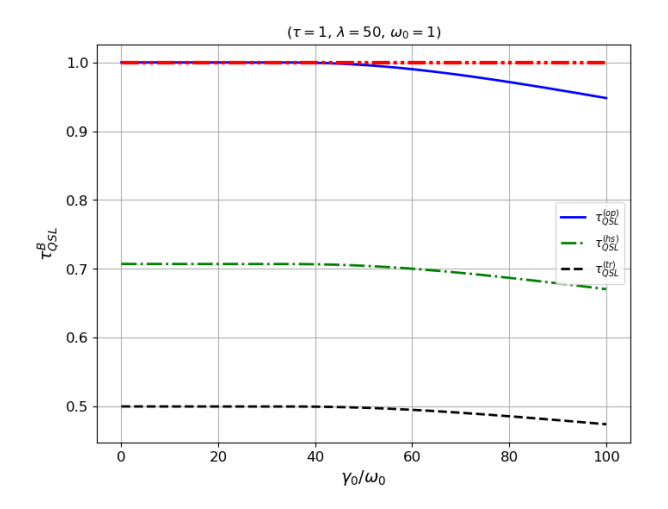


Figure 2. ML and MT QSLs  $\tau_{\rm QSL}^B$  given by Eq. (51), as a function of  $\gamma_0/\omega_0$  for the excited initial state given by  $\rho_0=|1\rangle\langle 1|$ . The evolution time was set as  $\tau=1,\lambda=50$ , and  $\omega_0=1$ . The horizontal dashed line represents the actual driving time  $\tau=1$ .

where  $\mu=1,\sqrt{2},2$  for the operator, Hilbert-Schmidt and trace norm, respectively.

Figures 1 and 2 show the quantum speed limit  $\tau_{\rm QSL}^B$ , given by equation (51), evaluated for the three different norms as a function of  $\gamma_0/\omega_0$ , for  $\tau=1$ , and for  $\lambda=20$  and  $\lambda=50$ , respectively. In agreement with equations (12) and (15), the MT-type QSL obtained from the Hilbert–Schmidt and the ML-type QSL obtained with the trace norm are looser than the ML-type QSL derived from the operator norm. As shown in the figures,  $\tau_{\rm QSL}^B$  exhibits a plateau over a relatively wide range of the parameter  $\gamma_0/\omega_0$ , after which the QSL decreases for larger values of  $\gamma_0/\omega_0$ . Moreover, the ML QSL corresponding to the operator norm becomes tight over a broad interval of  $\gamma_0/\omega_0$ , since it attains the actual evolution time  $\tau$  within that

range.

## B. Super-fidelity

Assuming that the system is in the initial state  $\rho_0$  given by equation (46), and using Eq. (25), we can write the ML-type QSL as

$$\tau_{\text{QSL}}^{s} = \frac{\frac{1}{2} \Big[ 1 - r_z - q_\tau(r_x^2 + r_y^2) + |q_\tau|^2 r_z (1 - r_z) - \kappa_1 \, \kappa_2^\tau \Big]}{\frac{1}{\tau} \int_0^\tau dt \, \frac{|\dot{q}_t|}{2} \, \sqrt{r_x^2 + r_y^2 + 4 (1 - r_z)^2 |q_t|^2} \, \left( 1 + \frac{\kappa_1}{\kappa_2^\tau} \right)}.$$

where

$$\begin{split} \kappa_1 & \doteq \sqrt{1 - r_x^2 - r_y^2 - r_z^2}, \\ \kappa_2^t & \doteq \sqrt{|q_t|^2 \Big( 2(1 - r_z) - (r_x^2 + r_y^2) - |q_t|^2 (1 - r_z)^2 \Big)}. \end{split}$$

If the initial state is taken as the excited state  $|1\rangle\langle 1|$  with added white noise, i.e.,  $\rho_0 = \frac{p}{2}\mathbb{I} + (1-p)\,|1\rangle\langle 1|$ , then in the basis  $\{|0\rangle\,, |1\rangle\}\,\,\tau_{\rm ost}^s$  can be written as

$$\tau_{\text{QSL}}^{s} = \frac{\frac{1}{2} \left[ (2-p) \left( 1 - (1-p)q_{\tau}^{2} \right) - \tilde{\kappa}_{1} \, \tilde{\kappa}_{2}^{\tau} \right]}{\frac{1}{\tau} \int_{0}^{\tau} dt \, (2-p) |q_{t}| \, |\dot{q}_{t}| \left( 1 + \frac{\tilde{\kappa}_{1}}{\tilde{\kappa}_{2}^{t}} \right)}$$
(52)

where

$$\begin{split} &\tilde{\kappa}_1 = \sqrt{p\left(2-p\right)}, \\ &\tilde{\kappa}_2^t = \sqrt{\left(2-p\right)|q_t|^2\left[2-\left(2-p\right)|q_t|^2\right]}. \end{split}$$

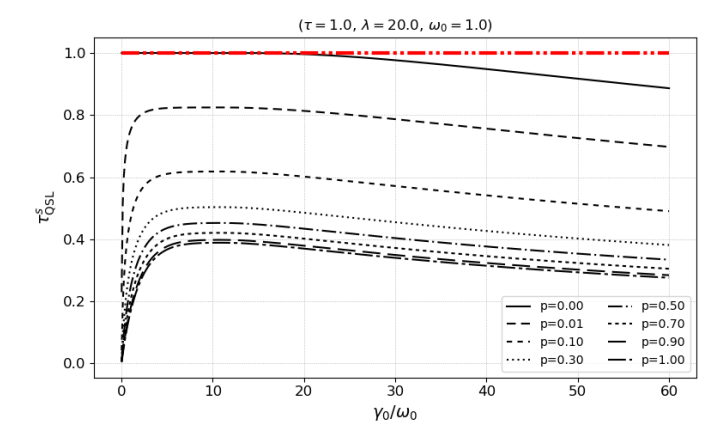


Figure 3. ML-type QSL  $\tau_{\rm QSL}^s$  given by Eq. (52), as a function of  $\gamma_0/\omega_0$  for different initial states of the form  $\rho_0=(p/2)\mathbb{I}+(1-p)|1\rangle\langle 1|$ . The evolution time was set as  $\tau=1, \lambda=20$ , and  $\omega_0=1$ . The horizontal dashed line represents the actual driving time  $\tau=1$ .

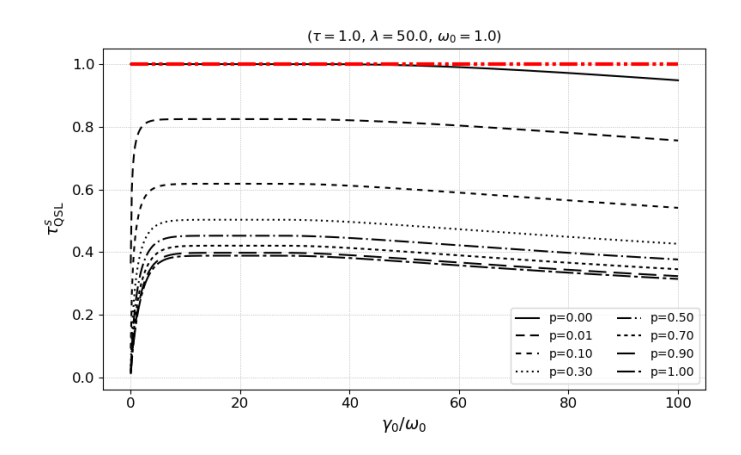


Figure 4. ML-type QSL  $\tau_{\rm QSL}^s$  given by Eq. (52), as a function of  $\gamma_0/\omega_0$  for different initial states of the form  $\rho_0=(p/2)\mathbb{I}+(1-p)\,|1\rangle\langle 1|$ . The evolution time was set as  $\tau=1,\,\lambda=50,$  and  $\omega_0=1.$  The horizontal dashed line represents the actual driving time  $\tau=1.$ 

Figures 3 and 4 show the ML-type QSL  $\tau_{\text{QSL}}^s$ , given by equation (52), evaluated for the operator norm as a function of  $\gamma_0$ , for  $\tau=1$ , and for  $\lambda=20$  and  $\lambda=50$ , respectively ( $\gamma_0$  is set in units of  $\omega_0$ ). In both figures, it can be observed that the ML-type QSL  $\tau_{\text{QSL}}^s$  is not tight for  $0< p\leq 1$ , as it never reaches the actual driving time  $\tau=1$ . For very small values of  $\gamma_0$  and  $0< p\leq 1$ , a rapid increase in  $\tau_{\text{QSL}}^s$  with a steep slope is observed at the beginning, until a plateau is reached for moderate values of  $\gamma_0$ . For larger values of the coupling constant,  $\tau_{\text{QSL}}^s$  decreases. As expected, since  $\mathcal{F}_s(\rho_0,\rho_\tau)$  reduces to the Bures fidelity  $F_B(\rho_0,\rho_\tau)$  for pure initial states, when p=0 (i.e.,  $\rho_0=|1\rangle\langle 1|$ ) the ML-type QSL  $\tau_{\text{QSL}}^s$  coincides with the ML-type QSL  $\tau_{\text{QSL}}^s$  corresponding to the operator norm, as shown in Figs. 1 and 2.

## C. Operator fidelity

Assuming that the system is in the initial state  $\rho_0$  given by equation (46), and using Eq. (36), we can write the MT-type QSL as

$$\tau_{\text{QSL}}^o = \frac{1 - \frac{1 + \vec{r} \cdot \vec{r}(\tau)}{\sqrt{(1 + |\vec{r}|^2)(1 + |\vec{r}(\tau)|^2)}}}{\frac{2}{\tau} \int_0^\tau \frac{|\dot{q}_t| \sqrt{r_x^2 + r_y^2 + 4(1 - r_z)^2 \, |q_t|^2}}{\sqrt{1 + |q_t|^2 (r_x^2 + r_y^2) + \left[1 - (1 - r_z)|q_t|^2\right]^2}} \, dt}.$$

where

$$\begin{split} |\vec{r}|^2 = & r_x^2 + r_y^2 + r_z^2, \\ \vec{r} \cdot \vec{r}(\tau) = & q_\tau (r_x^2 + r_y^2) + r_z - (r_z - r_z^2) |q_\tau|^2, \\ |\vec{r}(\tau)|^2 = & |q_\tau|^2 (r_x^2 + r_y^2) + \left[1 - (1 - r_z)|q_\tau|^2\right]^2. \end{split}$$

If the initial state is taken as  $\rho_0=\frac{p}{2}\mathbb{I}+(1-p)\,|1\rangle\!\langle 1|$ , then in this case  $au_{\text{OSL}}^o$  can be written as

$$\tau_{\text{QSL}}^{o} = \frac{1 - \frac{1 + (p-1)\left[1 - (2-p)q_{\tau}^{2}\right]}{\sqrt{\left(1 + (1-p)^{2}\right)\left(1 + \left[1 - (2-p)q_{\tau}^{2}\right]^{2}\right)}}}{\frac{2}{\tau} \int_{0}^{\tau} \frac{2(2-p)|q_{t}\dot{q}_{t}|}{\sqrt{1 + \left[1 - (2-p)q_{t}^{2}\right]^{2}}} dt} dt$$
(53)

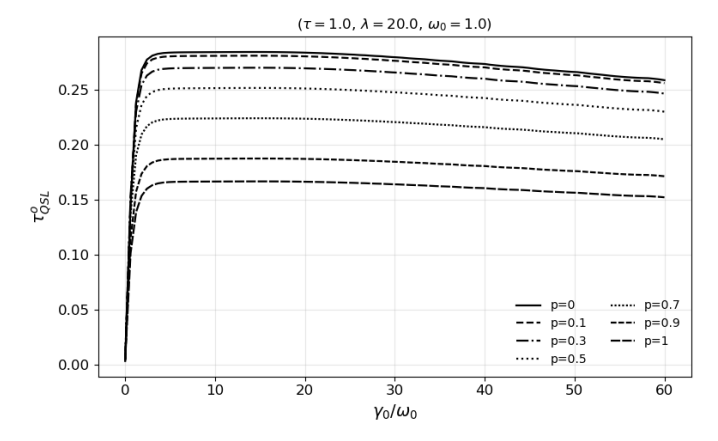


Figure 5. MT-type QSL  $au_{\text{QSL}}^{\circ}$  given by Eq.(53), as a function of  $\gamma_0/\omega_0$  for different initial states of the form  $\rho_0=(p/2)\mathbb{I}+(1-p)\,|1\rangle\!\langle 1|$ . The evolution time was set as  $\tau=1,\,\lambda=20,$  and  $\omega_0=1.$ 

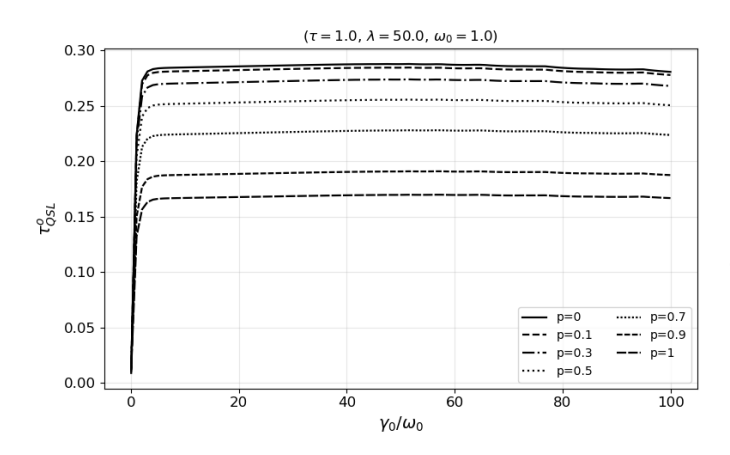


Figure 6. MT-type QSL  $au_{\text{QSL}}^{\circ}$  given by Eq.(53), as a function of  $\gamma_0/\omega_0$  for different initial states of the form  $\rho_0=(p/2)\mathbb{I}+(1-p)\,|1\rangle\!\langle 1|$ . The evolution time was set as  $\tau=1,\,\lambda=50,$  and  $\omega_0=1.$ 

Figures 5 and 6 show the MT-type QSL  $\tau_{\rm QSL}^o$ , given by equation (53), as a function of  $\gamma_0$ , for  $\tau=1$ , and for  $\lambda=20$  and  $\lambda=50$ , respectively. In both figures, it can be observed that the MT-type QSL  $\tau_{\rm QSL}^o$  is not tight as it never reaches the actual driving time  $\tau=1$ . As in the case of the ML-type QSL  $\tau_{\rm QSL}^s$ , for very small values of  $\gamma_0$  and  $0, a rapid increase in <math>\tau_{\rm QSL}^o$  with a steep slope is observed initially, until a plateau is reached for moderate values of  $\gamma_0$ . For larger values of the coupling constant  $\gamma_0$ ,  $\tau_{\rm QSL}^o$  decreases. In this case, it is worth noting that  $\mathcal{F}_o(\rho_0,\rho_\tau)$  does not reduce to the Bures fidelity  $F_B(\rho_0,\rho_\tau)$  for pure initial states, due to the additional

factor  $1/\sqrt{\text{Tr}\{\rho_t^2\}}$  (cf. Eq. (2)). Therefore, for p=0 (i.e.,  $\rho_0=|1\rangle\langle 1|$ ),  $\tau_{\text{\tiny QSL}}^o$  does not coincide with the  $\tau_{\text{\tiny QSL}}^B$  curves corresponding to the Hilbert–Schmidt norm, shown in Figs. 1 and 2.

#### D. Alternative fidelity

We shall assume the system to be in the initial state  $\rho_0$  given by equation (46). Using Eq. (5), the MT-type QSL can be written as

$$au_{ ext{ iny QSL}}^a = rac{1 - rac{1}{2}ig(1 + g_0 g_ auig)ig[1 + m{r}\cdotm{R}_ auig]}{rac{1}{ au}\int_0^ auig[T_1(t) + T_2(t) + T_3(t)ig]\,dt},$$

where

$$\begin{split} g_0 &\doteq \sqrt{\frac{1-r^2}{1+r^2}}, \\ g_t &\doteq \sqrt{\frac{1-R(t)^2}{1+R(t)^2}}, \\ \boldsymbol{r} &\doteq (r_x, r_y, r_z), \\ \boldsymbol{R}(t) &\doteq (r_x q_t, \ r_y q_t, \ 1 - (1-r_z) q_t^2), \\ T_1(t) &\doteq g_0 \, g_t^{-1} \, \left| \frac{\left[ \dot{\boldsymbol{R}}(t) \cdot \boldsymbol{R}(t) \right] \left[ 1 + \boldsymbol{r} \cdot \boldsymbol{R}(t) \right]}{\left[ 1 + R(t)^2 \right]^2} \right|, \\ T_2(t) &\doteq \sqrt{\frac{1}{4} (1+r^2) \, |\dot{\boldsymbol{R}}(t)|^2}, \\ T_3(t) &\doteq g_t \sqrt{\frac{1}{4} (1-r^2) \, |\dot{\boldsymbol{R}}(t)|^2}. \end{split}$$

and we define  $q_{\tau} \doteq q_t \big|_{t=\tau}$ ,  $\boldsymbol{R}_{\tau} \doteq \boldsymbol{R}(\tau)$ , and  $g_{\tau} \doteq g_t \big|_{t=\tau}$ . As before, we shall assume the initial state to be  $\rho_0 = \frac{p}{2}\mathbb{I} + (1-p)\,|1\rangle\langle 1|$ . In this case  $\tau_{\text{QSL}}^a$  can be written as

$$\tau_{\text{QSL}}^{a} = \frac{1 - \frac{1}{2} \left( 1 + \tilde{g}_{0} \tilde{g}_{\tau} \right) \left[ 1 + r_{z} R_{\tau} \right]}{\frac{1}{2\tau} \int_{0}^{\tau} |\dot{R}_{z}(t)| K(R_{z}(t); p) dt}, \tag{54}$$

with  $r_z = p - 1$ ,  $R_\tau = 1 - (2 - p)q_\tau^2$ ,

$$\tilde{g}_0 = \sqrt{\frac{1 - r_z^2}{1 + r_z^2}}, \qquad \tilde{g}_t = \sqrt{\frac{1 - R_z(t)^2}{1 + R_z(t)^2}},$$

and the weight function  $K(R_z; p)$  is given by

$$K(R_z; p) = \tilde{g}_0 g(R_z)^{-1} \frac{2 \left| R_z \left[ 1 + r_z R_z \right] \right|}{\left[ 1 + R_z^2 \right]^2} + \sqrt{1 + r_z^2} + g(R_z) \sqrt{1 - r_z^2},$$
 (55)

with

# $g(R_z) = \sqrt{\frac{1 - R_z^2}{1 + R_z^2}}.$

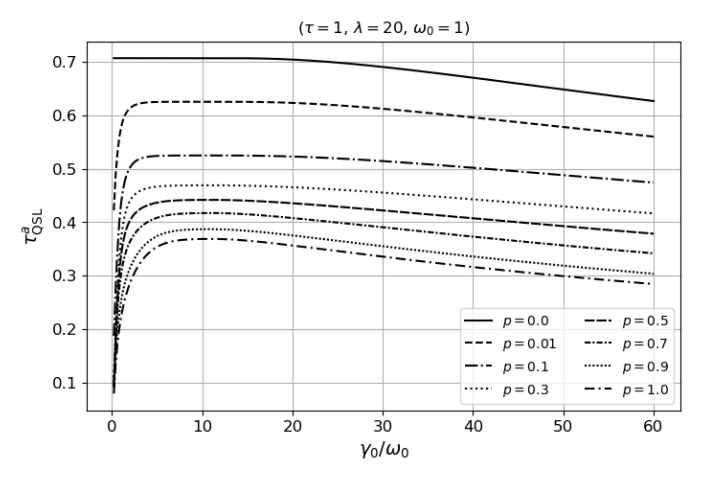


Figure 7. MT-type QSL  $au_{0\text{SL}}^a$  given by Eq.(54), as a function of  $\gamma_0/\omega_0$  for different initial states of the form  $\rho_0=(p/2)\mathbb{I}+(1-p)\,|1\rangle\!\langle 1|$ . The evolution time was set as  $\tau=1,\,\lambda=20$  and  $\omega_0=1$ .

Figures 7 and 8 show the MT-type QSL  $\tau_{\text{QSL}}^a$ , given by equation (54), as a function of  $\gamma_0/\omega_0$ , for  $\tau=1$ , and for  $\lambda=20$  and  $\lambda=50$ , respectively. It can be observed that the MT-type QSL  $\tau_{\text{QSL}}^a$  is not tight as it never reaches the actual driving time  $\tau=1$ . As in previous cases, for very small values of  $\gamma_0$  and  $0< p\leq 1$ , a rapid increase in  $\tau_{\text{QSL}}^a$  with a steep slope is observed initially, until a plateau is reached for moderate values of  $\gamma_0$ . For larger values of the coupling constant  $\gamma_0$ ,  $\tau_{\text{QSL}}^a$  decreases. As expected, since  $\mathcal{F}_a(\rho_0,\rho_\tau)$  reduces to the Bures fidelity  $F_B(\rho_0,\rho_\tau)$  for pure initial states,  $\tau_{\text{QSL}}^a$  coincides with the  $\tau_{\text{QSL}}^B$  curves corresponding to the Hilbert–Schmidt norm when p=0, as shown in Figs. 1 and 2.

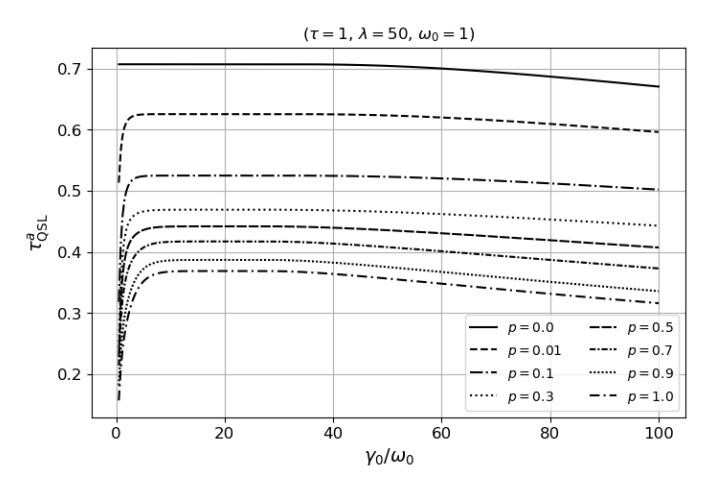


Figure 8. MT-type QSL  $au_{\rm osl}^a$  given by Eq.(54), as a function of  $\gamma_0/\omega_0$  for different initial states of the form  $\rho_0=(p/2)\mathbb{I}+(1-p)\,|1\rangle\!\langle 1|$ . The evolution time was set as  $\tau=1,\,\lambda=50$  and  $\omega_0=1$ .

#### VI. ANALYSIS AND DISCUSSION

#### A. Analytical results

Despite the apparent freedom in the choice of the function D(x) mentioned in Proposition 1 and in Theorems 1 through 6, it can be observed that all the derived QSLs ultimately depend only on the chosen fidelity and are independent of the specific form of D(x), provided that D(x) satisfies the properties stated in Proposition 1.

In the case of the Bures fidelity  $F_B$  Eq. (10) provides a ML-type QSL for closed quantum systems under time-dependent Hamiltonian evolution. In addition, Eq. (12) generalizes the ML-type QSL to arbitrary open system dynamics generated by positive time-local maps. Combining Eqs. (12) and (15), we obtain the unified QSL for Bures fidelity  $F_B$  as follows:

$$\tau_{\scriptscriptstyle \text{QSL}} = \max \left\{ \frac{1}{\mathcal{B}^{\scriptscriptstyle \text{(op)}}(\tau)}, \frac{1}{\mathcal{B}^{\scriptscriptstyle \text{(Tr)}}(\tau)}, \frac{1}{\mathcal{B}^{\scriptscriptstyle \text{(HS)}}(\tau)} \right\} \left[ 1 - F_B(\tau) \right],$$

which generalizes both the ML-type and MT-type QSLs to arbitrary open-system dynamics.

In the case of super fidelity, by combining Eqs. (25) and (28) we obtain n unified expression for the QSL as follows:

$$au_{ ext{QSL}} = \max \left\{ rac{1}{\mathcal{B}^{( ext{op})}( au)}, rac{1}{\mathcal{B}^{( ext{Tr})}( au)}, rac{1}{\mathcal{B}^{( ext{HS})}( au)} 
ight\} \left[ 1 - \mathcal{F}_s( au) 
ight].$$

Furthermore, the following inequality for trace-class operators holds [52]:

$$||A||_{\text{op}} \le ||A||_{\text{HS}} \le ||A||_{\text{Tr}}.$$
 (56)

Therefore,  $1/\mathcal{B}^{\text{\tiny (OP)}}(\tau) \geq 1/\mathcal{B}^{\text{\tiny (HS)}}(\tau) \geq 1/\mathcal{B}^{\text{\tiny (Tr)}}(\tau)$ , pointing out that the ML-type QSL using the operator norm should provide the sharpest estimate for the QSL time in all cases.

The Bures angle between a pure initial state and a final state represented by a general density operator, is given by:

$$\mathcal{L}(\rho_0, \rho_t) = \arccos\left(\sqrt{\langle \psi_0 | \rho_t | \psi_0 \rangle}\right),\tag{57}$$

where

$$F_B(\rho_0, \rho_t) = \langle \psi_0 | \rho_t | \psi_0 \rangle$$

can be identified as the Bures fidelity between an initial pure state  $\rho_0 = |\psi_0\rangle\langle\psi_0|$  and a general quantum state represented by the density operator  $\rho_t$ .

In a seminal work, Deffner et al. [15] used a geometric approach based on the Bures angle (see Eq. (57)) to derive MT and ML-type QSLs. They started their calculations by taking the time derivative of Eq. (57). Then, using von Neumann [15, 48–50] and Cauchy-Schwarz [15, 16] inequalities for operators, they arrived at a set of MT and ML-type QSLs. All of the obtained QSLs are written in terms of the Bures

angle [15]. However, it is worth mentioning that the metric character of the Bures angle is not needed at any point in their QSL derivation. Furthermore, working out all the QSLs obtained in Ref. [15], it can be seen that they can be rewritten in terms of Bures fidelity alone. On the other hand, all of their results can be reinterpreted and rewritten to express them in the form given by Theorem 2. Thus, all the QSLs obtained in Ref. [15] are contained within the framework introduced in our work. It is important to note again that the QSLs obtained in Ref. [15] are independent of the Bures angle and any other function of Bures fidelity,  $D(F_B)$ , that satisfies the properties stated in Proposition 1 and Theorem 2.

An approach similar to that used in Ref. [15] is used by Wu et al. in Ref. [37] where the so-called *modified Bures angle* is introduced:

$$\mathcal{L}_s(\rho_0, \rho_t) = \arccos\left(\sqrt{\mathcal{F}_s(\rho_0, \rho_t)}\right).$$
 (58)

In last equation,  $\mathcal{F}_s$  represents the *super fidelity* given by Eq. (1).

By taking the time derivative of Eq. (58) and using von Neumann and Cauchy inequalities for operators [15, 16, 48–50], Wu et al. [37] arrived at a set of MT and ML-type QSLs.

All of the obtained QSLs are written in terms of the quantity  $\mathcal{L}_s$  [37]. Again, all the QSLs obtained in Ref. [37] can be worked out, reinterpreted and rewritten to express them in the form given by Theorem 3. Thus, all the QSLs obtained in Ref. [37] are contained within the framework introduced in our work and, additionally, they are independent of the particular choice of  $\mathcal{L}_s$  and any other function  $D(\mathcal{F}_s)$  of the relative purity (cf. Eq. (1)) that satisfies the properties stated in Proposition 1 and Theorem 3.

# B. Numerical results

# 1. Bures fidelity

In order to analyze the behavior of  $\tau_{\text{QSL}}^B$  observed in Figs. 1 and 2, we shall examine equation (51) for different values of the coupling constant  $\gamma_0$ .

Let us define the excited-state population  $P_t \doteq |q_t|^2$ . Then, the denominator of (51) can be written as a *total variation* (i.e. path length) of  $P_t$  on  $[0, \tau]$ :

$$\frac{2\mu}{\tau} \int_0^{\tau} |q_t| \, |\dot{q}_t| \, dt = \frac{\mu}{\tau} \int_0^{\tau} |\dot{P}_t| \, dt.$$

The numerator is simply the net decay of the excited population over  $[0,\tau]$ :  $1-|q_{\tau}|^2=1-P_{\tau}$ . Hence

$$\tau_{\text{QSL}}^{B} = \frac{\tau}{\mu} \frac{1 - P_{\tau}}{\int_{0}^{\tau} |\dot{P}_{t}| dt}.$$
 (59)

Equation (59) shows that the qualitative behavior of  $\tau^B_{\rm QSL}$  is entirely controlled by the relation between the *net drop*  $1-P_{\tau}$  and the *accumulated path length*  $\int_0^{\tau} |\dot{P}_t| \, dt$ .

*Markovian regime: weak coupling*  $(0 < \gamma_0 \le \lambda/2)$ 

When  $\gamma_0 \leq \lambda/2$ , Eq. (48) implies  $q_t > 0$  and  $\dot{q}_t \leq 0$  for t > 0. Hence  $P_t = |q_t|^2$  is *strictly decreasing* on  $[0, \tau]$ , and therefore

$$\int_0^{\tau} |\dot{P}_t| \, dt = \int_0^{\tau} \left( -\dot{P}_t \right) dt = P_0 - P_{\tau} = 1 - P_{\tau}. \tag{60}$$

Inserting (60) into (59) we obtain the exact plateau:

$$\tau_{\text{QSL}}^B = \frac{\tau}{\mu}.\tag{61}$$

Thus, for fixed values of  $\tau$  and  $\lambda$ , the quantity  $\tau_{\rm QSL}^B$  remains constant throughout the Markovian region, taking the values  $\tau_{\rm QSL}^B = \tau$ ,  $\tau_{\rm QSL}^B = \tau/\sqrt{2}$ , and  $\tau_{\rm QSL}^B = \tau/2$ , for the operator norm, Hilbert–Schmidt norm, and trace norm, respectively. Physically, the state follows a *monotone* path from  $P_0=1$  to  $P_{\tau}$ ; the geometric "distance traveled" (denominator) equals the net drop (numerator) up to the prefactor  $\mu/\tau$ , so their ratio is the constant (61). This explains the observed *plateau* for  $\gamma_0 < \lambda/2$ .

non-Markovian regime: strong coupling ( $\gamma_0 > \lambda/2$ )

For  $\gamma_0 > \lambda/2$ , the amplitude is oscillatory under a decaying envelope:

$$q_t = e^{-\lambda t/2} \left[ \cos\left(\frac{h_2 t}{2}\right) + \frac{\lambda}{h_2} \sin\left(\frac{h_2 t}{2}\right) \right]$$
$$= A e^{-\lambda t/2} \cos\left(\frac{h_2 t}{2} - \delta\right),$$

with  $A=\sqrt{1+(\lambda/h_2)^2}$  and  $\delta=\arctan(\lambda/h_2)\in(0,\pi/2)$ . Consequently,  $P_t=|q_t|^2$  is *not* monotonic. The effective decay rate becomes time-dependent and oscillatory. Physically, information may transiently flow back from the environment to the system.

Because  $P_t$  is not monotonic, its *total variation* strictly exceeds the net drop:

$$\int_0^{\tau} |\dot{P}_t| \, dt > P_0 - P_{\tau} = 1 - P_{\tau},$$

whenever  $P_t$  has at least one local increase on  $[0, \tau]$ . From (59) this implies the strict inequality

$$au_{ ext{QSL}}^B < rac{ au}{\mu},$$

for  $\gamma_0 > \lambda/2$ , and at least one revival of  $P_t$  in  $(0,\tau)$ . This means that *non-Markovian oscillations* increase the path length in state space (the integral of  $|\dot{P}_t|$ ), while the net drop  $1-P_\tau$  remains bounded by the envelope. Thus, their ratio decreases below the plateau.

#### 2. Super fidelity

In order to analyze the behavior of  $\tau_{QSL}^s$  observed in Figs. 3 and 4, we shall examine equation (51) for different values of the coupling constant  $\gamma_0$ .

For the ML-type QSL with super-fidelity  $\mathcal{F}_s$ , we can write

$$au_{ ext{QSL}}^{s} = \frac{ ext{N}_{s}}{ ext{D}_{s}},$$

where

$$\begin{split} \mathbf{N}_s = & 1 - \mathcal{F}_s(\rho_0, \rho_\tau), \\ \mathbf{D}_s = & \frac{1}{\tau} \int_0^\tau \|\dot{\rho}_t\|_{\mathrm{op}} \left(1 + \sqrt{\frac{1 - \mathrm{Tr}\{\rho_0^2\}}{1 - \mathrm{Tr}\{\rho_t^2\}}}\right) dt. \end{split}$$

In this setting one obtains the compact forms

$$\begin{split} \mathbf{N}_s &= \frac{1}{2} \Big[ (2-p) \big( 1 - (1-p) q_\tau^2 \big) - \sqrt{p(2-p)} \times \\ & \sqrt{(2-p) \, q_\tau^2 \big( 2 - (2-p) q_\tau^2 \big)} \Big], \\ \mathbf{D}_s &= \frac{1}{\tau} \int_0^\tau (2-p) \, |q_t| |\dot{q}_t| \Bigg( 1 + \sqrt{\frac{p}{q_t^2 \big( 2 - (2-p) q_t^2 \big)}} \Bigg) dt. \end{split}$$

*Markovian regime: very weak coupling*  $(0 < \gamma_0 \ll \lambda)$ 

From the first branch of (48), a uniform small- $\gamma_0$  expansion yields

$$\begin{split} q(t) = &1 - \frac{\gamma_0}{2} \bigg[ t - \frac{1 - e^{-\lambda t}}{\lambda} \bigg] + O(\gamma_0^2), \\ \dot{q}(t) = &- \frac{\gamma_0}{2} \left( 1 - e^{-\lambda t} \right) + O(\gamma_0^2). \end{split}$$

Thus  $|q_t|=1+O(\gamma_0)$  and  $|\dot{q}_t|=O(\gamma_0)$ , monotonically increasing on  $[0,\tau]$ . Writing  $P_{\tau}\doteq |q_{\tau}|^2=1-\varepsilon+O(\gamma_0^2)$  with  $\varepsilon=O(\gamma_0)$ , and p>0 the super-fidelity numerator satisfies

$$N_s = \frac{1}{4} (2 - p) \left[ (2 - p) + \frac{(1 - p)^2}{p} \right] \varepsilon^2 + O(\varepsilon^3) = O(\gamma_0^2),$$

whereas the denominator obeys

$$D_{s} = \frac{(2-p)}{\tau} \int_{0}^{\tau} \gamma_{0} (1 - e^{-\lambda t}) dt + O(\gamma_{0}^{2}) = O(\gamma_{0}).$$

Therefore, for any fixed  $p \in (0, 1]$ ,

$$\tau_{\text{OSL}}^s(\gamma_0) = c(p, \lambda, \tau) \gamma_0 + O(\gamma_0^2),$$

i.e., it starts at zero and rises linearly with  $\gamma_0$ . For the special case p=0, the first-order cancellation disappears,  $N_s=O(\gamma_0)$  and  $D_s=O(\gamma_0)$ , and in the monotone sector one has the exact identity  $D_s=N_s/\tau$ , giving

$$\tau_{\text{OSL}}^s = \tau \quad (p = 0, \ \gamma_0 \le \lambda/2).$$

*Markovian regime: moderate coupling*  $(0 < \gamma_0 \le \lambda/2)$ 

When  $q_t$  decays monotonically and  $q_\tau \rightarrow 0$ ,

$$N_s \to \frac{2-p}{2},$$

$$D_s \to \frac{2-p}{\tau} \left(\frac{1}{2} + \frac{\sqrt{p}}{\sqrt{2}}\right),$$

so the ratio settles on the plateau

$$\tau_{\rm QSL}^s \, \approx \, \frac{\tau}{1+\sqrt{2p}} \, . \label{eq:tau_QSL}$$

non-Markovian regime: strong coupling ( $\gamma_0 > \lambda/2$ )

In this regime  $q_t$  becomes oscillatory and damped; using the second branch of (48) and

$$\dot{q}(t) = -e^{-\lambda t/2} \frac{\gamma_0 \lambda}{h_2} \sin\left(\frac{h_2 t}{2}\right),$$

the numerator remains near its endpoint-controlled plateau,  $N_s \approx (2-p)/2$ . In contrast, the denominator contains the *total variation*  $\int_0^\tau |\dot{q}_t| \, dt$ ; averaging the fast oscillations with slow envelope gives

$$D_s \propto \frac{\gamma_0}{h_2} \sim \sqrt{\frac{\gamma_0}{\lambda}} \qquad (\gamma_0 \gg \lambda),$$

yielding a characteristic decline

$$au_{ ext{QSL}}^s(\gamma_0) \ \sim \ C(p,\lambda, au) \, \sqrt{rac{\lambda}{\gamma_0}} \ \xrightarrow[\gamma_0 
ightarrow \infty]{} 0 \, .$$

# 3. Operator fidelity

From Eq. (53), the operator-fidelity QSL (MT-type) can be written as

$$\tau_{\text{QSL}}^o = \frac{N_o}{D_o},$$

where

non-Markovian regime: strong coupling ( $\gamma_0 > \lambda/2$ )

$$\begin{split} \mathbf{N}_{o} & \doteq \! 1 - \frac{1 + (p-1)u_{\tau}}{\sqrt{A(1+u_{\tau}^{2})}}, \\ \mathbf{D}_{o} & \doteq \! \frac{2}{\tau} \int_{0}^{\tau} \frac{2(2-p) \left| q_{t} \dot{q}_{t} \right|}{\sqrt{1+u_{t}^{2}}} \, dt. \end{split}$$

We also set

$$u_t \doteq 1 - (2 - p) q_t^2,$$
  
 $A \doteq 1 + (1 - p)^2.$ 

*Markovian regime: very weak coupling*  $(\gamma_0 \rightarrow 0^+)$ 

Expanding at fixed time (no short-time assumption),

$$q_t = 1 + \frac{\gamma_0}{\lambda} \left[ \frac{1 - e^{-\lambda t}}{2} - \frac{\lambda t}{2} \right] + O(\gamma_0^2),$$
  
$$\dot{q}_t = \frac{\gamma_0}{2} \left( e^{-\lambda t} - 1 \right) + O(\gamma_0^2).$$

Then  $u_{\tau}=(p-1)+\delta$  with  $\delta=-\frac{2-p}{\lambda}(1-e^{-\lambda\tau}-\lambda\tau)\gamma_0+O(\gamma_0^2)$ , and a Taylor expansion of N<sub>o</sub> around  $u_{\tau}=p-1$  gives

$$N_o = \frac{1}{2A^2} \, \delta^2 + O(\gamma_0^3) = C_F(p, \lambda, \tau) \, \gamma_0^2 + O(\gamma_0^3), \quad C_F > 0,$$

while  $D_o = \frac{(2-p)}{\sqrt{A}} \gamma_0 \lambda \tau + O(\gamma_0^2)$ . Hence

$$\tau_{\scriptscriptstyle \mathrm{QSL}}^o(\gamma_0) = \frac{\mathrm{N}_o}{\mathrm{D}_o} = C(p,\lambda,\tau)\,\gamma_0 + O(\gamma_0^2),$$

i.e. it starts at zero and increases linearly with  $\gamma_0$ .

*Markovian regime: moderate coupling*  $(0 < \gamma_0 \le \lambda/2)$ 

Here  $q_t$  is real, nonnegative and decreasing; using  $|q_t\dot{q}_t|=-\frac{1}{2}\frac{d}{dt}(q_t^2)$  and  $u=1-(2-p)q^2$  yields the *exact* denominator

$$\mathbf{D}_o = \frac{2}{\tau} \Big[ \operatorname{arsinh}(u_\tau) - \operatorname{arsinh}(p-1) \Big].$$

As  $\gamma_0$  grows (for fixed  $\lambda, \tau$ ),  $q_{\tau} \to 0$  so  $u_{\tau} \to 1$ , and both

$$N_o \rightarrow 1 - \frac{p}{\sqrt{2A}},$$

$$D_o \rightarrow \frac{2}{\tau} \left[ \operatorname{arsinh}(1) - \operatorname{arsinh}(p-1) \right]$$

saturate, producing the observed plateau in  $\tau_{osl}^o$ .

Now  $q_t$  oscillates with frequency  $h_2$  and decays as  $e^{-\lambda t/2}$ . The factor  $\gamma_0 \lambda/h_2 \sim \sqrt{\gamma_0 \lambda/2}$  and the sin term boost the time-averaged  $|\dot{q}_t|$ , thus increasing  $D_o$ , while oscillatory revivals can place  $\rho_\tau$  closer to  $\rho_0$ , so  $N_o$  saturates or decreases. Consequently,  $\tau_{\rm QSL}^o$  decreases after the plateau (with small ripples, as shown in Figs. 5 and 6).

# 4. Alternative fidelity

From Eq. (54), the alternative–fidelity QSL (MT-type) can be written as

$$au_{\scriptscriptstyle ext{QSL}}^a = rac{ ext{N}_a}{ ext{D}_a},$$

where

$$\mathbf{N}_{a} \doteq 1 - \frac{1}{2} \left( 1 + \tilde{g}_{0} \tilde{g}_{\tau} \right) \left[ 1 + \mathbf{r} \cdot \mathbf{R}_{\tau} \right] 
\mathbf{D}_{a} \doteq \frac{1}{2\tau} \int_{0}^{\tau} |\dot{R}_{z}(t)| K(R_{z}(t); p) dt,$$
(62)

In this case the function  $D_a$  can be written as a weighted path length along the z-axis of the Bloch sphere. The function  $K(R_z;p)$  is nonnegative (cf. (55)) and depends only on the Bloch coordinate  $R_z$  and the mixing parameter p; it is the same in all regimes discussed below.

*Markovian regime:* very weak coupling  $\gamma_0 \to 0^+$ 

In the limit  $\gamma_0 \to 0^+$  (with  $\lambda$  and  $\tau$  fixed), the system remains very close to its initial state for all times  $t \leq \tau$ . In this regime  $\mathcal{F}_a(\rho_0,\rho_\tau)$  admits the expansion  $\mathcal{F}_a(\rho_0,\rho_\tau) = 1 - C(p,\tau) \, \gamma_0^2 + \mathcal{O}(\gamma_0^3)$ , so that  $N_a \sim \gamma_0^2$  as  $\gamma_0 \to 0^+$ . At the same time, the evolution of the Bloch coordinate  $R_z(t)$  is very slow and  $R_z(t) \simeq r_z$  for all  $t \in [0,\tau]$ . As a consequence, one can approximate the weight in Eq. (62) by  $K(R_z(t);p) \simeq K(r_z;p)$ , with

$$K(r_z; p) = g_0 g(r_z)^{-1} \frac{2 |r_z [1 + r_z^2]|}{[1 + r_z^2]^2} + \sqrt{1 + r_z^2} + g(r_z) \sqrt{1 - r_z^2},$$

and  $|\dot{R}_z(t)| \propto \gamma_0$ , implying  $D_a \sim \gamma_0$ . Hence,

$$au_{ ext{QSL}}^a(\gamma_0) = rac{ ext{N}_a}{ ext{D}_a} \sim \gamma_0, \qquad \gamma_0 o 0^+.$$

Thus, the quantum speed limit starts from zero and increases approximately linearly with the coupling strength in the very weak-coupling Markovian regime. In this limit the function  $K(R_z;p)$  is effectively evaluated at the initial Bloch point  $R_z=r_z$ .

*Markovian regime: moderate coupling*  $0 < \gamma_0 \lesssim \lambda/2$ 

For moderate Markovian couplings  $(\gamma_0 \leq \lambda/2 \text{ and } \gamma_0 \tau \gtrsim 1)$ , the excited-state population decays significantly within the interval  $[0,\tau]$ , and the evolution of the Bloch coordinate is well approximated by  $R_z(t) = 1 - (2-p)e^{-\Gamma t}$ , with an effective decay rate  $\Gamma \propto \gamma_0$ . As  $\gamma_0$  increases in this window, the final value  $R_z(\tau)$  rapidly approaches 1, so that  $\rho_\tau \simeq |0\rangle\langle 0|$  and  $\mathcal{F}_a(\rho_0,\rho_\tau)$  saturates to  $\mathcal{F}_a(\rho_0,\rho_\tau) \to \mathrm{Tr}(\rho_0\,|0\rangle\langle 0|) = p/2$ . Hence, the numerator approaches the constant

$$N_a(p) \simeq 1 - \frac{p}{2}.\tag{63}$$

In the same Markovian approximation, the monotonicity of  $R_z(t)$  allows us to change variables in Eq. (62) from t to  $R_z=R_z(t)$ , which yields

$$D_a(\gamma_0) = \frac{1}{2\tau} \int_{R_z = p-1}^{R_z = R_z(\tau)} K(R_z; p) dR_z,$$
 (64)

with  $K(R_z;p)$  defined in Eq. (55). As  $R_z(\tau) \to 1$  for increasing  $\gamma_0$ , the integral in Eq. (64) saturates to the purely geometric quantity

$$D_a(p,\tau) \simeq \frac{1}{2\tau} \int_{p-1}^1 K(R_z; p) dR_z,$$

which is independent of  $\gamma_0$  (within the Markovian approximation). Consequently, in this intermediate regime both the distance encoded in  $N_a$  and the path length encoded in  $D_a$  become nearly coupling-independent, and

$$\tau_{\mathrm{QSL}}^{a}(\gamma_{0}) \simeq \tau_{\mathrm{QSL}}^{a}(p,\tau) = \frac{2\tau \left(1 - \frac{p}{2}\right)}{\int_{p-1}^{1} K(R_{z}; p) dR_{z}},$$

which appears as the plateau region in the numerical plots. Here the function  $K(R_z;p)$  weights the different points along the straight segment in Bloch space connecting the initial Bloch coordinate  $R_z=p-1$  with the ground state  $R_z=1$ .

*Non-Markovian regime: strong coupling*  $\gamma_0 > \lambda/2$ 

When  $\gamma_0 > \lambda/2$ , the dynamics enter the non-Markovian regime and the amplitude  $q_t$  acquires oscillatory contributions. Accordingly,  $R_z(t) = 1 - (2 - p)q_t^2$  becomes oscillatory as a function of time, with a number of oscillations within  $[0,\tau]$  that increases with  $\gamma_0$ . In the parameter range considered here, the endpoint  $R_z(\tau)$  remains close to 1 even for strong couplings, so that the numerator  $N_a$  stays approximately equal to its plateau value  $N_a(p)$  (cf. (63)).

In contrast, the denominator retains the path-length structure

$$D_a(\gamma_0) = \frac{1}{2\tau} \int_0^\tau |\dot{R}_z(t)| K(R_z(t); p) dt,$$

with the same weight  $K(R_z;p)$  as in the Markovian analysis. In the non-Markovian regime, every oscillation of  $R_z(t)$  adds an extra positive contribution to the total variation  $\int_0^\tau |\dot{R}_z(t)| \, dt$ , and therefore to  $D_a(\gamma_0)$ . As  $\gamma_0$  increases, the total path length grows, while the endpoint-based distance  $N_a$  remains essentially constant. Consequently,

$$au_{ ext{QSL}}^a(\gamma_0) = rac{ ext{N}_a(\gamma_0)}{ ext{D}_a(\gamma_0)} \quad ext{decreases for } \gamma_0 > \lambda/2,$$

in agreement with the numerical observation that the plateau region in  $au_{\mathrm{QSL}}^a$  is followed by a decay in the strongly non-Markovian regime. The same local weight  $K(R_z;p)$  governs all three regimes; what changes with  $\gamma_0$  is the geometry of the trajectory  $R_z(t)$  through the Bloch space.

## 5. Comparative QSLs analysis

For a pure initial state of the form  $\rho_0=|1\rangle\langle 1|$ , the ML-type QSL  $\tau_{\rm QSL}^B$  built with the operator norm is tight in the Markovian regime, since on that interval it coincides with the driving time  $\tau$  (here,  $\tau=1$  in the referenced figure). In the non-Markovian regime, i.e., in the strong-coupling domain  $\gamma_0>\lambda/2$ , non-Markovian effects can increase the time–averaged generator norm (information backflow), and consequently the value of  $\tau_{\rm QSL}^B$  drops below its Markovian value. These observations are in complete agreement with the results reported in [15].

The *qualitative* behavior of  $\tau_{\text{QSL}}^s$ ,  $\tau_{\text{QSL}}^o$ , and  $\tau_{\text{QSL}}^a$  curves across the different coupling regimes determined by  $\gamma_0$  is similar. For  $0 , the QSL curves exhibit an approximately linear increase for <math>0 < \gamma_0 \ll \lambda$ , followed by a plateau for moderate couplings  $\gamma_0 < \lambda/2$ , and subsequently a decrease for  $\gamma_0 > \lambda/2$ , over the ranges displayed in the figures. These trends can be explained from the closed forms derived for the various QSLs. As expected, for  $\tau_{\text{QSL}}^s$  with  $0 , the tightest QSL is obtained when the operator norm is used. Moreover, since super fidelity <math>\mathcal{F}_s(\rho_0, \rho_t)$  reduces to the Bures fidelity  $F_B(\rho_0, \rho_t)$  when the initial state is pure, i.e.,  $\rho_0 = |1\rangle\langle 1|$  in the scenario analyzed, the  $\tau_{\text{QSL}}^s$  curve computed with  $\mathcal{F}_s(\rho_0, \rho_t)$  and the operator norm *coincides* with the curve for  $\tau_{\text{QSL}}^{s}$  (with Bures fidelity) with the operator norm; see Figs. 1 and 2, as anticipated.

For mixed initial states of the form  $\rho_0 = \frac{p}{2}\mathbb{I} + (1-p)\,|1\rangle\langle 1|$ , the QSLs  $\tau_{\text{QSL}}^o$ , and  $\tau_{\text{QSL}}^a$  are looser than  $\tau_{\text{QSL}}^s$  when the operator norm is used. This behavior is expected, because  $\tau_{\text{QSL}}^o$  and  $\tau_{\text{QSL}}^a$  are MT-type QSLs and, in general, are not tight. Since  $\mathcal{F}_a(\rho_0,\rho_t)$  coincides with the Bures fidelity  $F_B(\rho_0,\rho_t)$  when the initial state is pure (that is, when p=0 and  $\rho_0=|1\rangle\langle 1|$  in this scenario), the QSL  $\tau_{\text{QSL}}^a$  reduces to the MT-type Bures QSL  $\tau_{\text{QSL}}^B$  when the Hilbert-Schmidt norm is employed, as expected. By contrast,  $\mathcal{F}_o(\rho_0,\rho_t)$  does not reduce to  $F_B(\rho_0,\rho_t)$  for pure  $\rho_0$  due to the additional factor  $1/\sqrt{\text{Tr}(\rho_t^2)}$  in  $F_o$  (cf. Eq. (2)); therefore, for p=0 one has that  $\tau_{\text{QSL}}^o$  does not reduce to  $\tau_{\text{QSL}}^B$  when the Hilbert-Schmidt norm is used, again as expected.

Unlike the results presented in Ref. [15]—which strictly applies when the initial state  $\rho_0$  is pure—the use of generalized fidelities such as  $\mathcal{F}_s(\rho_0,\rho_t)$ ,  $\mathcal{F}_o(\rho_0,\rho_t)$ , and  $\mathcal{F}_a(\rho_0,\rho_t)$  allows us to propose QSLs that are applicable when the initial state  $\rho_0$  is *mixed*. Although the QSLs derived from  $\mathcal{F}_s(\rho_0,\rho_t)$ ,  $\mathcal{F}_o(\rho_0,\rho_t)$ , and  $\mathcal{F}_a(\rho_0,\rho_t)$  are in general not tight, they provide nontrivial constraints on the evolution time in the mixed-state setting, which constitutes a meaningful extension of the geometric approach explored here. All of our qualitative conclusions are fully consistent with Ref. [15], and with subsequent analyses of QSLs based on  $\mathcal{F}_s(\rho_0,\rho_t)$ ,  $\mathcal{F}_o(\rho_0,\rho_t)$ , and  $\mathcal{F}_a(\rho_0,\rho_t)$  for mixed initial states of the form  $\rho_0=\frac{p}{2}\mathbb{I}+(1-p)|+\rangle\langle+|$  with  $|+\rangle=(|0\rangle+|1\rangle)/\sqrt{2}$  (see, e.g., Refs. [37, 43, 53]).

#### VII. CONCLUDING REMARKS

We have analyzed the role of functionals of generalized fidelity measures in the derivation of quantum speed limits (QSLs) within a geometric framework. We have demonstrated that any monotone and differentiable reparametrization of the selected fidelity produces identical ML/MT-type bounds, thereby rendering the QSL invariant under such transformations and providing a unified perspective connecting fidelity- and metric-induced geometric formulations. This invariance clarifies the inherent limitations of attempts to improve QSLs through functional transformations of fidelity and indicates that meaningful advances must instead arise from alternative fidelity definitions. The general structure developed in this work reveals that, once a particular generalized fidelity is specified, the corresponding ML- and MT-type bounds for both unitary and nonunitary (Lindblad-type) dynamics depend exclusively on that choice of fidelity measure. Furthermore, we have shown that various QSLs previously reported in the literature naturally emerge as particular instances of our framework (e.g., [15, 37, 43, 53, 55]), suggesting a coherent and general foundation upon which further developments—based on other generalized fidelity measures—may be constructed. Moreover, the results presented here can be straightforwardly extended by considering generalized fidelity measures beyond those employed as illustrative examples in the present study.

Using the damped Jaynes-Cummings (DJC) model as a concrete physical setting, we verified that, for a *pure* ini-

tial state  $\rho_0 = |1\rangle\langle 1|$  (as in Ref. [15]), the Bures fidelitybased ML-type QSL with the operator norm is tight throughout the Markovian regime ( $\gamma_0 \leq \lambda/2$ ), yielding a plateau at the actual driving time  $\tau$ . Upon entering the non-Markovian regime ( $\gamma_0 > \lambda/2$ ), the time dependence of the decay rate interpretable as information backflow-increases the timeaveraged generator norm, so the Bures fidelity-based ML-type QSL decreases below its Markovian value; this plateau-anddecrease trend is fully consistent with the results presented in Ref. [15] (cf. Sec. VA). For the generalized fidelities  $\mathcal{F}_s(\rho_0, \rho_t)$  (super-fidelity, cf. Eq. (1)),  $\mathcal{F}_o(\rho_0, \rho_t)$  (operator fidelity as defined here, cf. Eq. (2)), and  $\mathcal{F}_a(\rho_0, \rho_t)$  (alternative fidelity, cf. Eq. (3)), the qualitative dependence of the QSL on the coupling strength is similar across regimes: an approximately linear rise for  $0 < \gamma_0 \ll \lambda$ , a plateau for moderate coupling  $\gamma_0 < \lambda/2$ , and a decrease for  $\gamma_0 > \lambda/2$  (cf. Secs. VB, VC, and VD). In the case of  $\mathcal{F}_s(\rho_0, \rho_t)$  and for 0 ,the operator norm yields the tightest QSLs; moreover, since  $\mathcal{F}_s(\rho_0,\rho_t)$  coincides with the Bures fidelity for pure  $\rho_0$ , the QSL obtained from  $\mathcal{F}_s(\rho_0, \rho_t)$  with the operator norm reproduces the Bures fidelity-based ML-type QSL with the operator norm when  $\rho_0 = |1\rangle\langle 1|$ , in complete agreement with [15]. For mixed initial states of the form  $\rho_0 = \frac{p}{2}\mathbb{I} + (1-p)|1\rangle\langle 1|$ , the QSLs derived from  $\mathcal{F}_o(\rho_0,\rho_t)$  and  $\mathcal{F}_a(\rho_0,\rho_t)$  are looser than those from  $\mathcal{F}_s(\rho_0, \rho_t)$  under the operator norm, in line with their MT-type character and the general non-tightness of such QSLs. Moreover, our results indicate that the MTtype QSLs obtained by means of  $\mathcal{F}_o(\rho_0, \rho_t)$  are looser than the corresponding MT-type QSLs derived from  $\mathcal{F}_a(\rho_0, \rho_t)$ , in complete agreement with Ref. [43]. Crucially, while the Bures fidelity-based QSLs are directly applicable to pure initial states, the use of  $\mathcal{F}_s(\rho_0, \rho_t)$ ,  $\mathcal{F}_o(\rho_0, \rho_t)$ , and  $\mathcal{F}_a(\rho_0, \rho_t)$ extends the geometric QSL approach analyzed in this work to mixed initial states, providing nontrivial—albeit generally non-tight—QSLs.

## ACKNOWLEDGMENTS

T.M.O, M. P. and P.W.L are fellows of the National Research Council of Argentina (CONICET). Y. A. has a fellowship from CONICET. The authors are grateful to CONICET (PIP N°: 135/23), Secretaria CyT-UNLP (Proyecto 11/X959), and Secretaria de Ciencia y Técnica de la Universidad Nacional de Córdoba (SeCyT-UNC, Argentina, Proyecto Consolidar 2023-2025) for financial support.

<sup>[1]</sup> L. Mandelstam and I. Tamm, J. Phys. (USSR) 9, 249 (1945).

<sup>[2]</sup> N. Margolus and L. B. Levitin, Physica D 120, 188 (1998).

<sup>[3]</sup> G. N. Fleming, Nuovo Cimento A 16, 232 (1973).

<sup>[4]</sup> K. Bhattacharyya, J. Phys. A 16, 2993 (1983).

<sup>[5]</sup> J. Anandan and Y. Aharonov, Phys. Rev. Lett. 65, 1697 (1990).

<sup>[6]</sup> L. Vaidman, Am. J. Phys. 60, 182 (1991).

<sup>[7]</sup> J. Uffink, Am. J. Phys. 61, 935 (1993).

<sup>[8]</sup> D. C. Brody, J. Phys. A 36, 5587 (2003).

<sup>[9]</sup> P. Pfeifer, Phys. Rev. Lett. **70**, 3365 (1993).

<sup>[10]</sup> V. Giovannetti, S. Lloyd, and L. Maccone, Phys. Rev. A 67, 052109 (2003).

<sup>[11]</sup> S. Luo, Physica D 189, 1 (2004).

<sup>[12]</sup> L. B. Levitin and T. Toffoli, Phys. Rev. Lett. 103, 160502 (2009)

<sup>[13]</sup> S. Morley-Short, L. Rosenfeld, and P. Kok, Phys. Rev. A 90, 062116 (2014).

- [14] N. Hörnedal, and O. Sönnerborn, Phys. Rev. Res. 5, 043234 (2023).
- [15] S. Deffner and E. Lutz, Phys. Rev. Lett. 111, 010402 (2013).
- [16] A. del Campo, I. L. Egusquiza, M. B. Plenio, and S. F. Huelga, Phys. Rev. Lett. 110, 050403 (2013).
- [17] F. Campaioli, F. A. Pollock, F. C. Binder, and K. Modi, Phys. Rev. Lett. 120, 060409 (2018).
- [18] M. M. Taddei, B. M. Escher, L. Davidovich, and R. L. de Matos Filho, Phys. Rev. Lett. 110, 050402 (2013).
- [19] F. Campaioli, F. A. Pollock, and K. Modi, Quantum 3, 168 (2019)
- [20] K. Funo, N. Shiraishi, and K. Saito, New J. Phys. 21, 013006 (2019)
- [21] E. O'Connor, G. Guarnieri, and S. Campbell, Phys. Rev. A 103, 022210 (2021).
- [22] D. Thakuria, A. Srivastav, B. Mohan, A. Kumari, and A. K. Pati, J. Phys. A: Math. Theor. 57, 025302 (2024).
- [23] N. Hörnedal, O. A. Prośniak, A. del Campo, and A. Chenu, Quantum 9, 1729 (2025).
- [24] A. Srivastav, V. Pandey, B. Mohan, and A. K. Pati, arXiv:2406.08584 [quant-ph] (2025).
- [25] Z.-y. Mai and C.-s. Yu, Phys. Rev. A 108, 052207 (2023).
- [26] Z.-y. Mai, Z. Liu, and C.-s. Yu, Quantum 9, 1774 (2025).
- [27] Z.-y. Mai and C.-s. Yu, Phys. Rev. A 112, 052205 (2025)
- [28] A. del Campo, A. Grabarits, D. Makarov, and S.-H. Shinn, arXiv:2506.21672 [quant-ph] (2025).
- [29] N. Mirkin, F. Toscano, and D. A. Wisniacki, Phys. Rev. A 94, 052125 (2016).
- [30] P. J. Jones and P. Kok, Phys. Rev. A 82, 022107 (2010).
- [31] M. Zwierz, Phys. Rev. A 86, 016101 (2012).
- [32] D. Paiva Pires, M. Cianciaruso, L. C. Céleri, G. Adesso, and D. O. Soares-Pinto, Phys. Rev. X 6, 021031 (2016).
- [33] K. Lan, S. Xie, and X. Cai, New J. Phys. 24, 055003 (2022)

- [34] D. J. C. Bures, Tran. Amer. Math. Soc. 135, 199 (1969).
- [35] A. Uhlmann, Rep. Math. Phys. 9, 273 (1976).
- [36] R. Jozsa, J. Mod. Opt. 41, 2315 (1994).
- [37] S.-X. Wu and C.-S. Yu, Sci. Rep. 10, 5500 (2020).
- [38] M. A. Nielsen and I. L. Chuang, *Quantum Computation and Quantum Information*, (Cambridge, Cambridge, 2000).
- [39] T. M. Osán and P. W. Lamberti, Phys. Rev. A 87, 062319 (2013).
- [40] J. A. Miszczak, Z. Puchala, P. Horodecki, A. Huhlmann and Życzkowski, Quantum Inf. Comput. 9, 0103 (2009).
- [41] P. E. M. F. Mendonça, R. d. J. Napolitano, M. A. Marchiolli, C. J. Foster, and Y. C. Liang, Phys. Rev. A 78, 052330 (2008).
- [42] X. Wang, C-S. Yu and X.X. Yi, Phys. Lett. A 373 (2008) 58–60
- [43] A. Ektesabi, N. Behzadi and E. Faizi, Phys. Rev. A 95, 022115 (2017).
- [44] G. Lindblad, Commun. Math. Phys. 48, 119 (1976).
- [45] V. Gorini, A. Kossakowski, and E. C. G. Sudarshan, J. Math. Phys. 17, 821 (1976).
- [46] H.-P. Breuer and F. Petruccione, *The Theory of Open Quantum Systems*, (Oxford, Oxford, 2007).
- [47] R. Bhatia, Matrix Analysis, (Springer, Berlin, 1997).
- [48] J. von Neumann, Tomsk Univ. Rev. 1, 286 (1937).
- [49] L. Mirsky, Monatshefte für Math. **79**, 303 (1975).
- [50] R. D. Grigorieff, Math. Nachr. 151, 327 (1991).
- [51] The trace, Hilbert-Schmidt and operator norms correspond to  $p = 1, 2, \infty$ , respectively.
- [52] B. Simon, *Trace Ideals and Their Applications*, 2nd ed. (American Mathematical Society, Providence, 2005).
- [53] Z. Sun, J. Liu, J. Ma and X. Wang, Sci. Rep. 5, 8444 (2015).
- [54] H.-P. Breuer, B. Kappler, and F. Petruccione, Phys. Rev. A 59, 1633 (1999).
- [55] S.-X. Wu and C.-S. Yu, Phys. Rev. A 98, 042132 (2018).